ARTICLE **Communicated by Noah Cowan**

Estimating Phase From Observed Trajectories Using the Temporal 1-Form

Simon Wilshin
swilshin@rvc.ac.uk
Royal Vet College, London NW1 OTU, UK

Matthew D. Kvalheim
kvalheim@umbc.edu
University of Maryland, Baltimore County, MD 21250, USA

Clayton Scott
clayscot@umich.edu
Shai Revzen
shrevzen@umich.edu
University of Michigan, Ann Arbor, MI 41089, USA

Oscillators are ubiquitous in nature and are usually associated with the existence of an asymptotic phase that governs the long-term dynamics of the oscillator. We show that the asymptotic phase can be estimated using a carefully chosen series expansion that directly computes the phase response curve (PRC) and provides an algorithm for estimating the coefficients of this series. Unlike previously available data-driven phase estimation methods, our algorithm can use observations that are much shorter than a cycle; has proven convergence rate bounds as a function of the properties of measurement noise and system noise; will recover phase within any forward invariant region for which sufficient data are available; recovers the PRCs that govern weak oscillator coupling; and recovers isochron curvature and recovers nonlinear features of isochron geometry. Our method may find application wherever models of oscillator dynamics need to be constructed from measured or simulated time-series.

1 Introduction: Phase as an Organizing Principle

Oscillatory dynamics are at the foundation of neuroscience (Hoppensteadt & Izhikevich, 1997; Wodeyar et al., 2021), but oscillators appear in virtually every physical science—for example, in coupled oscillations of predator and prey populations (May, 1972); in control theory (Monga et al., 2019); in chemistry (Epstein & Pojman, 1998); in physics (Głazek & Wilson, 2002); and in electrical (Van der Pol, 1934), civil (Duffing, 1918), and mechanical (Stoker, 1950) engineering. When oscillations are robustly stable

Neural Computation **37, 2158–2204** (2025) © 2025 Massachusetts Institute of Technology
https://doi.org/10.1162/neco.a.32

Downloaded from http://direct.mit.edu/neco/article-pdf/37/12/2158/2554618/neco.a.32.pdf by Ramona Marchand on 07 December 2025

under perturbations, the underlying mathematical structure of oscillators shares many properties across all these cases. One of the most significant of these properties is the existence of a simple asymptotic phase that encodes the long-term outcome of any (recoverable) perturbation.

We have discovered that by representing phase as a Temporal 1-Form, we could bring to bear interpolation tools from machine learning to allow an asymptotic phase to be computed in a data-driven way directly from time series of noisy measurements without a need to know or estimate the governing equations. This would allow investigators to perform phase reduction directly from experimental measurements, and thereby construct reduced models of oscillatory systems and how these systems couple to each other. In this article, we present our algorithm applied to animal locomotion data, simulations with known ground truth, some classical neural oscillator models—the Fitzhugh-Nagumo oscillator (FitzHugh, 1961; Nagumo et al., 1962) and other oscillators from the literature, including the Selkov oscillator (Sel'Kov, 1968).

Several recent methods of phase estimation rely on fully estimating the equations of motion, for example, using RNN-s (Cestnik & Abel, 2019), a modern twist on an approach that harkens back at least to 1990 (Kostelich & Yorke, 1990) and used a KNN-based affine model for estimating dynamics. Similar approaches that rely on fully modeling the dynamics include rectifying the entire dynamics into a classical, Floquet (1883), a normal form using the parameterization method (Pérez-Cervera & Huguet, 2020) or phase and isostable modeling (Wilson, 2020; Wilson & Ermentrout, 2018). These approaches attempt to perform full data-driven Floquet analysis (Revzen & Kvalheim, 2015, 2016; Revzen, 2009), on the dynamics in a region around the limit cycle.

Our goals are more modest, closer to the goals of Mauroy et al., (2013) and Mauroy and Mezić (2018), in that we do not attempt to reconstruct the entire dynamics. However, unlike these Koopman-based modeling approaches, we take an inherently nonlinear approach to our estimation problem. Our more modest goals come with a simpler estimation procedure, which also allows us to provide bounds on the rate of convergence of our loss function. This provides a unique and novel result: a phase estimation method that has a computable statistical power allowing experimental protocols that use our algorithm to be designed and evaluated with quantifiable accuracy.

In applying this definition of asymptotic phase to stochastic differential equations and showing that as an appropriate low-noise limiting case, the deterministic asymptotic phase is recovered, we also wade into the wider discussion of generalizing phase to stochastic oscillatory systems (Schwabedal & Pikovsky, 2013; Thomas & Lindner, 2014; Cao et al., 2020; Engel & Kuehn, 2021; also see Pikovsky, 2015, and Thomas & Lindner, 2015, for a spirited discussion).

Downloaded from http://direct.mit.edu/neco/article-pdf/37/12/2158/2554618/neco.a.32.pdf by Ramona Marchand on 07 December 2025

2 Definition of an Oscillator

Mathematical models in the physical sciences frequently use differential equations of order 1 or higher. Newton's laws, and the equations governing electrical circuits are usually written as second-order systems, $\ddot{x} = g(x, \dot{x})$, whereas first order systems,

$$\dot{x} = f(x), \tag{2.1}$$

govern chemical reactions and ecological population dynamics, for example. Here x is a state of the system, description of the system sufficiently specific to yield a unique future outcome. By rewriting the second-order equations in terms of positions and velocities (or momenta), the former can be reduced to a special case of the latter, and we will therefore consider first-order systems. We will consider only systems that admit a unique solution for all time, along with more technical requirements specified in sections A.3 and A.4.

Sometimes dynamical systems have periodic solutions to $\dot{x} = f(x)$. We consider the case that the curve traced by such a solution attracts nearby solutions. More specifically, we consider only the typical case that this convergence occurs at an exponential rate (which is equivalent to the periodic solution being normally hyperbolic); for brevity, we will call these limit cycles. We use the term *oscillator* to describe the dynamics $f(\cdot)$ restricted to the set of initial conditions that, after a sufficiently long relaxation period, converge arbitrarily close to a designated limit cycle. That set of initial conditions that evolve toward the limit cycle is termed the "stability basin" of the limit cycle or the domain of the oscillator.

Once the system settles on (or arbitrarily near) the limit cycle, it oscillates with the same pattern repeatedly, allowing points from this closed curve to be invertibly mapped onto the unit circle so that the images on the circle cycle at a constant angular rate ω. This angle is what is commonly referred to as the phase (angle) of the oscillator at that state.

This phase can be naturally extended to the entire stability basin thanks to the following observation: all initial conditions converge to the limit cycle, but points on the limit cycle forever remain apart. To model the long-term behavior of an oscillator, we could represent each off-cycle point by a point on the cycle that most closely represents its long-term behavior, constructing a "phase map" $\mathrm{P}(\cdot)$. When convergence to the limit cycle is at an exponential rate, such long-term representatives exist and are unique. By extension, the phase angle of the representative can be taken to be the phase angle of all the points it represents.

Since we can assign to every point in our stability basin a phase angle, we can divide up the stability basin into sections (hypersurfaces) with the same phase. In the mathematics literature, these are called isochrons.

Downloaded from http://direct.mit.edu/neco/article-pdf/37/12/2158/2554618/neco.a.32.pdf by Ramona Marchand on 07 December 2025

Isochrons are smooth surfaces (manifolds) and therefore have no cusps or kinks; however, this fact is a nontrivial result (Guckenheimer, 1975). For a D-dimensional system, the isochrons will be a set of $D-1$ dimensional (i.e., co-dimension 1) hypersurfaces on each of which phase is constant. This implies that in a Euclidean space, the (vector) derivative of phase is perpendicular to the isochrons. These derivatives at the points of the limit cycle govern the long-term sensitivity of the system to small perturbations and are called the phase response curves (PRCs). In the study of linear time periodic (LTP) systems, these are also sometimes called the phase-dependent impulse response functions (ϕIRFs) (Rafiee & Kiemel, 2020). They provide a complete first-order description of the long-term responses of the oscillator to small perturbations, but degrade to failure in describing the phase response to perturbations as the perturbations become large enough to be affected by the curvature of the isochrons.

3 A Subtle Problem with Phase Estimation

Naively, it would seem that phase can be taken to be a real number, for example, in the interval $[0, 2\pi)$, and using modern function estimation tools, we could define a loss function that guides an optimization to converge onto a phase map.

The defining property of phase is that it is time-like; loosely stated, a real-valued phase ϕ satisfies $\phi(x(t)) = \omega t + \phi(x(0))$, where x is a state of the oscillator and the period of the oscillator is $2\pi/\omega$. This is obviously true on the limit cycle, but extends to all trajectories of the oscillator (see section A.4). Thus, we could seek to fit a real-valued function that maintains this property everywhere else, using something like the integral of $1 - \cos(\phi(x(s+t)) + \phi(x(s)) - \omega t)$ over pairs of trajectory points as a loss function.

Such optimizations encounter several obstacles. Real-valued phase is only defined up to an arbitrary constant. Furthemore, the stated defining property of phase only defines phase up to a constant when applied to a domain that contains the whole limit cycle and is otherwise suitable (forward invariant), but the same condition leaves phase underconstrained when these conditions are not met. The consequnce of these obstacles is that the phase function cannot be built piecemeal: as an optimization consolidates a notion of phase in different highly sampled parts of state-space, those partial functions might end up disagreeing by arbitrary constants wherever their domains overlap. Stitching together partial functions by adding a suitable correction offset only works to a point, since multiple partial functions can be merged together and then become impossible to resolve when the merging operations try to produce a domain that extends around a full cycle and closes on itself.

A natual approach toward avoiding this problem could be to switch to finding the gradient of phase. Since the gradient is the same for functions

Downloaded from http://direct.mit.edu/neco/article-pdf/37/12/2158/2554618/neco.a.32.pdf by Ramona Marchand on 07 December 2025

that differ by a constant, such a gradient would be unique. Unfortunately, no real-valued phase is continuous, and thus phase is not everywhere differentiable. The discontinuity is obvious on the limit cycle itself, where once the trajectory closes back on itself, the phase value should be 2π, but the phase of that point has already been assigned to be 0. However, because the gradient of every choice of real-valued phase is defined everywhere in the oscillator except where this wrap-around discontinuity appears, we can be assured that a gradient can be extended to the discontinuity either by taking the limit of surrounding gradient values or by filling in the value from the gradient of a different real-valued phase whose discontinuity occurs elsewhere. Informally, this "gradient" is the Temporal 1-Form, which we denote $d\phi$, and its estimation is the main topic of this article.

The defining property of $d\phi$ is that $d\phi(x) \cdot f(x) = \omega$, as would follow from the fact that (abbreviating x for $x(t)$ where unambigous)

$$\frac{d}{dt}\left[\phi(x(t)) - \phi(x(0))\right] = \omega = \nabla_x \phi(x) \cdot \dot{x} = \nabla\phi(x) \cdot f(x) =: d\phi(x) \cdot f(x), \quad (3.1)$$

wherever $\nabla\phi(x)$ is defined. We distinguish $\nabla\phi(\cdot)$ from $d\phi(\cdot)$ in that $d\phi(\cdot)$ is a 1-form that is defined everywhere, whereas our use of $\nabla\phi(\,\cdot\,)$ is informal, $\nabla\phi(\,\cdot\,)$ is not everywhere defined, and its use is merely meant to invoke the reader's familiarity with the chain rule for scalar functions.

The problem of fitting $d\phi(\,\cdot\,)$ from data is somewhat easier: the solution is unique, and the defining property is a local one; we can seek to minimize a loss such as the integral of $|d\phi(x) \cdot \dot{x} - \omega|^2$ on the data points. However, many different (co-)vector fields will have the same inner product with $f(\,\cdot\,)$ at a point x, including vector fields that cannot arise as gradients. In fact, vector fields that can arise as gradients of a local real-valued function are precisely those whose Jacobian is symmetric, a result known as the Poincaré lemma. We might thus hope to estimate $d\phi(\,\cdot\,)$ by combining basis functions that are themselves gradients, thereby ensuring that the result will be a gradient.

Here we would encounter the same loop-closing obstacle as before in a changed and more obvious form. $d\phi(\,\cdot\,)$ is not a gradient of any real-valued function and therefore cannot be represented as a sum of gradients. This can be seen easily from the fact that going once around the limit cycle, the path integral of $d\phi(\,\cdot\,)$ should be 2π, whereas the path integral of a gradient on a closed loop must be zero from the fundamental theorem of calculus.

Algebraic topologists have explored and resolved this conundrum of vector fields that are locally gradient-like but not globally a gradient in the study of differential forms (see section A.2) and the de Rham cohomology. From de Rham's results, we can learn that in the stability basin of an oscillator, the collection of gradient-like vector fields and the collection of vector fields that are actually gradients differ by a one-dimensional family. In particular, the difference of any two gradient-like vector fields whose

Downloaded from http://direct.mit.edu/neco/article-pdf/37/12/2158/2554618/neco.a.32.pdf by Ramona Marchand on 07 December 2025

closed-loop integral on the limit cycle is equal will always be a vector field that is an actual gradient of some scalar function.

This insight, formally that the first de Rham cohomology of the stability basin of any oscillator is the ring of real numbers," implies that by subtracting a gradient-like vector field whose closed-loop integral on the limit cycle is equal to 2π, we can obtain a new gradient-like vector field that is an actual gradient. We can then reconstruct this residual vector field from gradients with local support using conventional function estimation tools. This is what our algorithm does.

The Temporal 1-Form (section A.3 for a definition) is unique for each oscillator, is mathematically equivalent to other representations of asymptotic phase (see theorem 1 in section A.4), and can be approximated using our algorithm with roughly the same statistical efficiency as the law of large numbers for data sampling and system and measurement noise (see theorems 2 and 3 and remark 3 in section A.5). This provable convergence property is unique among all data-driven phase-estimation algorithms we are aware of.

4 Our Algorithm

Our algorithm takes as input pairs $(x_k, \dot{x}_k)\, k = 1 \ldots N$ of observed states and state velocities, and learns both an angle-valued function that takes states to phase and a matching vector valued function giving the Temporal 1-Form.

In broad strokes, we perform our algorithm as follows. First, we construct a limit cycle estimate and rectify the data by constructing a smooth change of coordinates that maps an estimated limit cycle to the unit circle at a constant angular rate. Then we subtract this constant circulation and express the remainder using vector-valued basis functions (all in the rectified coordinates). We select the basis function coefficients by minimizing the cost of a loss function that is zero for the residual produced from the true Temporal 1-Form. The basis functions we use here are derivatives of known scalar-valued functions. The sum of the scalar-valued functions and the phase angle contribution of the circulation is our resulting phase estimate.

4.1 Rectification. The first step of our algorithm is reminiscent of Phaser from Revzen and Guckenheimer (2008) in that it estimates the limit cycle and computes a phase estimate that evolves uniformly on that limit cycle estimate. We differ from Revzen and Guckenheimer (2008) in that we do not rely on the existence of trajectory segments in the data at all; this possibility was mentioned in Revzen and Guckenheimer (2008) but discarded due to the superior performance of Hilbert transform-derived pseudo-phases. Here we use a pseudo-phase derived from a principal component analysis (PCA) projection of the data, allowing the use of data points regardless of whether there are any prior or following points on the same trajectory.

Downloaded from http://direct.mit.edu/neco/article-pdf/37/12/2158/2554618/neco.a.32.pdf by Ramona Marchand on 07 December 2025

In addition to rectifying the pseudo-phase to evolve uniformly in time in a manner reminiscent of Phaser here, we also rectify the shape of the limit cycle to the two-dimensional unit circle on the plane of the first two principal components of the data and express this transformation as a computable diffeomorphism.

In particular, we translate the data to zero mean, then use PCA on the positions x_k to rotate the two major covariance axes into the first two coordinates. We assume that in these new coordinates, the trajectories wind around the origin at rates that do not hugely vary,[1] and those data are mostly constrained to an annulus in this 2D circulation plane comprising the first two coordinates. Data that do not meet these assumptions would require preprocessing before being used some other transformation, more elaborate than PCA, would be needed to bring data to meet the circulation requirement, and some rate transformation might be needed to bring the circulation rates that do not vary too extremely.

Consider the data in cylindrical coordinates: scalar angle θ and radius r for the circulation plane and Cartesian z with the remaining coordinates of each data point (see Figure 1A showing such data). We fit Fourier series $\hat{r}(\theta)$ and $\hat{z}(\theta)$ to the data, and thereby constructed an approximate model of the limit cycle. This also allowed us to estimate the period T as the rate of circulation of this limit cycle model. Using a similar approach to Phaser (Revzen & Guckenheimer, 2008), we constructed a map $\hat{\phi}(\theta)$ so that $\left|2\pi t/T - (\hat{\phi} + \theta)\right|^2$ is minimized. We extended this map to a mapping taking the input x coordinates to rectified coordinates,

$$(\theta, r, z) \mapsto (\theta - \hat{\phi}(\theta), r/\hat{r}(\theta), z - \hat{z}(\theta)), \tag{4.1}$$

which rectifies the data to motion on the unit circle (see Figure 1B) at close to a constant angular rate (see Figure 1C). We refer to the state x in its rectified coordinates by the symbol q.

4.2 Approximation by Topologically Motivated Basis Functions. We reconstructed the Temporal 1-Form by a series approximation using a basis.[2] Most of the forms comprising this basis were themselves derivatives of real-valued functions; we refer to this as basis forms.

Unfortunately, it is not possible to reconstruct the Temporal 1-Form from any linear combination of basis forms, for reasons outlined in section 3,

[1] We have tested our algorithm with some relaxation oscillators with convincing results. Nevertheless, there is no theoretical guarantee that the limit cycle estimate will converge if the timescale disparities are too extreme.

[2] We use the term *basis* informally, as it is used, for example, in the notion of radial basis functions in machine learning, to mean a collection of functions whose finite linear spans are dense in the function space of interest.

Downloaded from http://direct.mit.edu/neco/article-pdf/37/12/2158/2554618/neco.a.32.pdf by Ramona Marchand on 07 December 2025

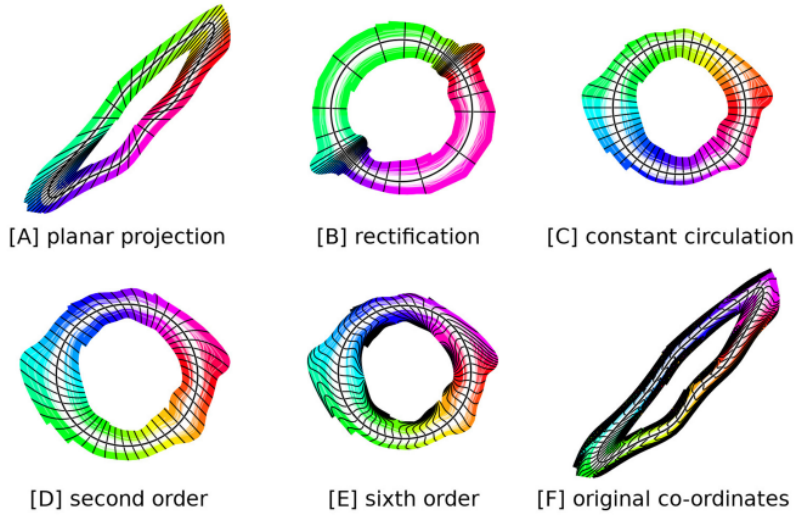


Figure 1: Steps of the algorithm, showing phase (as color; isochrons as contours), trajectories (white traces), and a limit cycle estimate (dark line) as applied to a randomly generated simulation system (see section A.1 for how test data were generated). We projected the data down to their two principal components and then built a limit cycle model from the polar angle in the circulation plane (A). Using this, we rectified the radius to the unit circle (B) and then rectified the phase to a constant circulation rate (C). We then added basis terms (up to order 2 (D), order 6 (E)) and converted the resulting series approximation back to the original coordinates (F). These results compare favorably with the known ground-truth phase.

which we now restate in the technical language of differential forms. A differential form, which is gradient like in the sense of section 3, "closed"; written as a vector field, its Jacobian would be symmetric. A differential form that is the exterior derivative ("gradient") of a scalar function is "exact." The Temporal 1-Form is closed but not exact. The study of de Rham cohomology from algebraic topology teaches us that on the basin of attraction associated with an oscillator, any two closed 1-forms a, b can be related as $a = \omega b + \mathbf{d}c$ for some ω real and $\mathbf{d}c$ an exact 1-form that is the exterior derivative of a scalar-valued function c. In particular, the Temporal 1-Form of all oscillators on a given domain differs by a scale—the units used to measure phase along one complete cycle—and some additional part that is always a derivative of a scalar function.[3] Thus, it is enough to find any 1-form b that has a nonzero integral on $\Gamma \subset \mathbf{M}$, the image of the limit cycle. Once found, it is

[3] We are deeply indebted to Dan Guralnik for pointing out this insight on the de Rham cohomology of oscillators. That this insight extends from $\mathcal{C}^\infty$ closed forms (used in

Downloaded from http://direct.mit.edu/neco/article-pdf/37/12/2158/2554618/neco.a.32.pdf by Ramona Marchand on 07 December 2025

straightforward to compute ω and express the difference $d\phi - \omega b$ using the basis forms. The b we chose comes from finding a 2D projection of the oscillator such that no point maps to the 2D origin but Γ encloses the origin. The (exterior) derivative of the polar angle of the projection will then have all the requisite properties.

Our approximation algorithm proceeds by optimizing the parameters (detailed in Table 1) of

$$\begin{aligned} d\phi(\theta, r, z) &:= d\theta + \sum_{\nu} m_\nu \mathbf{d} v_\nu(\theta, r, z) \\ \nu &:= (i, j, k)\ \ 0 \le i \le n-2,\ \ j, k \in \mathbb{N}; \\ v_{\nu(i,j,k)}(\theta, r, z) &:= \xi_i(z)\rho_j(r)u_k(\theta) \end{aligned} \tag{4.2}$$

as indicated by the following expression, where the constant C is selected to be consistent with the previously computed period:

$$\arg\min_{d\phi} \sum_i \left(d\phi(x_i), \dot{x}_i - C\right)^2. \tag{4.3}$$

Here we have multiple observations of state and its derivative, $(x, \dot{x})$, and, hence, x and $\dot{x}$ have an index, i. First, working in the rectified coordinates q, we selected a scale for $d\theta(q)$ such that $\int_\Gamma d\theta(q)$ is the period of oscillation.

To find the remaining coefficients m_ν we solved

$$\arg\min_{m_\nu, C} \sum_{\nu, i} \left(m_\nu \mathbf{d} v_i(q_i), \dot{q}_i - (C - d\theta(q_i), \dot{q}_i)\right)^2. \tag{4.4}$$

We note that equation 4.4 is a conventional ordinary least squares regression problem, and thus m_ν can be solved for using standard tools. Note that $\mathbf{d} v_i(q_i)$ is formed from a sum of products of these basis terms, meaning it is not a separable function of z,r and θ. The order of the expansion used is determined by the limits of the sum for v_ν in Table 1.

The contribution of individual Fourier-polynomial terms can be seen in Figure 2.

We have made the code for this algorithm available at https://purl.archive.org/birds-lab/code/formphase.git, along with the examples at https://purl.archive.org/birds-lab/code/formphaseexamples.git.

de Rham cohomology) to C^0 closed forms follows from general results on smoothing currents (de Rham, 1984, pp. 61–70); alternatively, it is not difficult to give a direct proof of this result for oscillators.

Downloaded from http://direct.mit.edu/neco/article-pdf/37/12/2158/2554618/neco.a.32.pdf by Ramona Marchand on 07 December 2025

Table 1: Basis Forms and Their Integrals in Rectified Coordinates θ, r, z.

Name	Integral	Differential 1-form	
Angle	$\theta \approx \arctan2(q_0, q_1)$ *(no global integral exists)*	$d\theta$	(4.5)
Fourier	$u_k(\theta) := a_k \cos(k\theta) + b_k \sin(k\theta)$	$\mathbf{d}u_k(\theta) = ka_k \sin(k\theta)d\theta - kb_k \cos(k\theta)d\theta$	(4.6)
Polynomial	$\rho_j(r) := (r-1)^j$	$\mathbf{d}\rho_j(r) = j(r-1)^{j-1}\mathbf{d}r$	(4.7)
Out of plane	$\xi_i(z) := z_i$ for $i > 0$, or 1, for $i = 0$	$\mathbf{d}\xi_i(z) = \mathbf{d}z_i$ for $i > 0$, or 0, for $i = 0$	(4.8)

Notes: The general $d\phi$ structure is in equation 4.4. After the rectification step, $d\theta$ is a trivial expression (equation 4.5), and provides the circulation needed to ensure that remaining terms can be exact—the sum of derivatives $\mathbf{d}v_\nu$. The v_ν basis functions are a first-order expansion in z, via equation 4.8, a Fourier expansion in θ via equation 4.6, and a polynomial (see equation 4.7) expansion in r. Note that ν is uniquely determined by i, j, and k.

Downloaded from http://direct.mit.edu/neco/article-pdf/37/12/2158/2554618/neco.a.32.pdf by Ramona Marchand on 07 December 2025

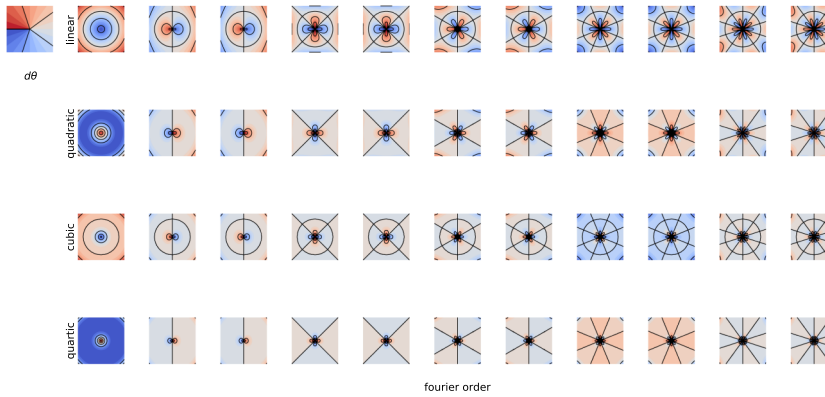


Figure 2: A plot of $u_k(\theta)\rho_j(r)$ terms for orders up to five. From left to right, the order of the Fourier term increases and the cosine and sine terms alternate. From top to bottom, we have increasing order of the radial polynomial. In the top left corner is the $d\theta$ term, so labeled as linear, quadratic, cubic, and quartic.

5 Performance of the New Algorithm

5.1 Convergence and Statistical Power. Since our goal is to estimate the Temporal 1-Form of a nondeterministic system subject to measurement noise, it is of great importance to obtain some bounds on convergence rate. The precise definitions, theorems, and proofs are in supplemental material A.5, whereas here, we discuss the terms contributing to these bounds in a more informal sense.

First, consider the inherent limitations of any such estimation procedure. Our data come as a sample of $(x_i, \dot{x}_i)$ from some underlying measure, μ defining what states x_i are observable using the experimental system. States that cannot be observed to evolve to the limit cycle because they go through a nonobservable region of state space, are effectively outside the stability basin and have no meaningful phase; thus one important limitation is that only the forward invariant parts of the support of μ (which perforce must include the limit cycle) can have a well-defined answer.

Second, consider a measurement noise η_i defined by $\dot{x}_i := f(x_i) + \eta_i$. Obviously, even if we repeatedly sample the same exact point (i.e., x_i is constant), the convergence of our estimate of $f(x_i)$ will depend on the noise distribution of η_i, and so some properties of convergence under this noise are needed. We will assume that the strong law of large numbers applies: the sample variance of η_i converges to its second moment, which is bounded by κ, and we describe the convergence of our algorithm in terms of an upper bound on the sample variance of η_i, $\zeta(N)$.

Downloaded from http://direct.mit.edu/neco/article-pdf/37/12/2158/2554618/neco.a.32.pdf by Ramona Marchand on 07 December 2025

Third, consider that to drive our convergence, we optimize against a loss function $J(\cdot)$, because it is computed from noisy data, would have some error ϵ even when applied to the true Temporal 1-Form $d\phi$. We use ϵ as the bound for how badly noise η_i interacts with the loss function computation to corrupt its results.

Fourth, consider that even if we had some desirable, achievable estimate $\widehat{d\phi}$ approximating the true $d\phi$, we are attempting to construct $\widehat{d\phi}$ from a sampling process with its own reconstruction error with some convergence rate $\xi(N)$.

Finally, the magnitude of the Temporal 1-Form itself plays a role in the magnitude of the error and the loss function. We assume a bound M_0 uniformly bounding both the true $d\phi$ and its estimate $\widehat{d\phi}$.

In terms of these quantities, we have two main convergence results.

Theorem 2 shows that under broad conditions (given in section A.5.1)

$$\sqrt{\| J_N\left(\widehat{d\phi}_N\right) \|_\infty} \leq \left(4 + 2\sqrt{2}\right) M_0 \sqrt{\kappa} + 2\sqrt{\epsilon},$$

that is, the loss function error vanishes as $\kappa \to 0$ and $\epsilon \to 0$.

Theorem 3 shows that for the constant c from lemma 4,

$$c \left\| \widehat{d\phi}_N - d\phi \right\|_\infty^2 \leq \xi(N) + 4\left[\left(2 + \sqrt{2}\right) M_0 \zeta(N) + \sqrt{\epsilon}\right]^2,$$

that is, the estimated Temporal 1-Form after a sample of N points, $\widehat{d\phi}_N$, converges to the true $d\phi$, and how quickly and tightly it does so is bounded by the limits and rates of $\xi(\cdot)$ and $\zeta(\cdot)$.

It should be noted our formulation of noise allows for describing both measurement and system noise (see remark 1).

5.2 Performance on 2D, 3D, and 8D Simulations. We used the approach described in section A.1 to produce three randomly generated simulation systems of dimension 2, 3, and 8, each consisting of a stochastic oscillator with known convergence rates embedded into the state-space using a randomly generated H-map diffeomorphism.[4] The first is easy to visualize; the second is the minimal dimension in which general eigenvalues can appear in the Floquet structure; the third is more typical of the dimensionality of biological systems for which we developed this estimation method. We examined the performance of three different estimates of the phase of these systems and compared the estimated phase to the ground truth provided by θ of equation A.3.

[4] Our method of generating random diffeomorphisms with closed-form Jacobians and inverses may be of independent interest for testing numerical methods. We thank John Guckenheimer for the key ideas that led to the random H-map algorithm.

Downloaded from http://direct.mit.edu/neco/article-pdf/37/12/2158/2554618/neco.a.32.pdf by Ramona Marchand on 07 December 2025

The first phase estimator we used is comparable to event-based phase estimates commonly used in biological research. Researchers often use distinguished events, such as voltage levels in the nervous system (Danner et al., 2015), footfall (Ting et al., 1994; Jindrich & Full, 2002), or anterior extreme position of a limb (Cruse & Schwarze, 1988) to identify the beginning of a cycle and presume that phase evolves uniformly in time between these events. As our event, we used the zero crossing of the first principal component of the data. The second phase estimator we used was our previously published Phaser algorithm (Revzen & Guckenheimer, 2008). The third phase estimator was derived from the Temporal 1-Form as described in this article, and is referred to as form phase. A visualization of the steps in the execution of the form-phase estimation algorithm is depicted in Figure 1.

We wish to estimate phase, in the practical sense of its use as a reduced-order model, from experimental data that resemble the sample paths of a stochastic differential equation. To validate our results, we trained our phase estimation methods on one set of simulated sample paths and tested them on another, generated from the same stochastic dynamical system. We calculated a model residual by subtracting the ground-truth phase from the estimated phases obtained with each method. We removed the trial-to-trial indeterminate phase offset by taking the circular mean of the model residual to be zero.

The simulations use three different varieties of noise. Our models satisfy a stochastic differential equation of the form:

$$dx = f(x)\,dt + d\eta, \tag{5.1}$$

where $d\eta$ is a nonlinear noise term. We introduce three varieties of noise. The first is the variability in the initial condition, that is, $x(0)$. Our initial positions are shifted from the limit cycle along a random direction whose length is drawn from a gaussian of zero mean and standard deviation equal to that shown in Table 2.

The two remaining varieties of noise are a phase noise and a nonlinear stochastic term. We simulated 100 trajectories with 955 samples per trajectory, with full details of how initial conditions were selected and how these terms were implemented in the integrator provided in sections A.1.3 and A.1.4. As our system is constructed with a ground-truth phase, we can rewrite it in coordinates that include phase. The phase noise term adds a gaussian of mean zero with standard deviation given in Table 2. The final noise term, the system noise, is a nonlinear stochastic term. For this we generate a new H-map of the same dimension as the system and transform a gaussian stochastic process through this map. The process has mean zero, and the unscaled standard deviation is also given in Table 2.

The simulations along with the code used to generate them are available at https://purl.archive.org/birds-lab/code/hmaposc.git. The results show that the form phase method has lower mean-square residuals than

Downloaded from http://direct.mit.edu/neco/article-pdf/37/12/2158/2554618/neco.a.32.pdf by Ramona Marchand on 07 December 2025

Table 2: Variance of Residual Phase for Different Phase Estimation Techniques with Different Initial Condition Noise and System Noise Levels.

	Noise			Residual Variance		
D	Initial	System	Phase	Event	Phaser	Form
2	0.1	0.01	0.1	0.128	0.0473	0.0185
2	0.2	0.01	0.1	0.127	0.0456	0.0205
2	0.1	0.02	0.1	0.135	0.0480	0.0199
2	0.1	0.01	0.2	0.222	0.0885	0.0389
3	0.066	0.0066	0.066	0.102	0.156	0.0164
3	0.133	0.0066	0.066	0.102	0.0920	0.0189
3	0.066	0.0133	0.066	0.108	0.0863	0.0214
3	0.066	0.0066	0.133	0.159	0.0897	0.0252
8	0.025	0.0025	0.025	0.0789	0.0232	0.0340
8	0.05	0.0025	0.025	0.0776	0.0246	0.0455
8	0.025	0.005	0.025	0.0816	0.0352	0.0671
8	0.025	0.0025	0.05	0.0889	0.0273	0.0460

Note: A description of how these noise terms were implemented is given in section A.1.4.

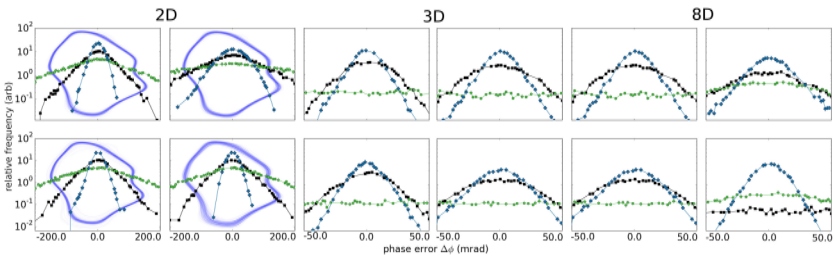


Figure 3: Comparison of phase estimators on 2D, 3D, and 8D systems by relative frequency of phase error; for the 2D system, a plot of the trajectories of this system is included in blue in the background. Comparison of event phase (green) Phaser (black), and form phase (turquoise) noise distributions on simulated trajectories. Plots show four different conditions for each dimension: one baseline condition (top left), an increase in the magnitude of the stochastic diffusion term (top right), an increase in the levels of variability in the initial conditions (bottom left), and an increase in noise on the coordinate corresponding to phase in the equivalent deterministic system (bottom right; see Table 2, these different sources of variability are described in detail in section A.1.4).

the Phaser method, which in turn has lower mean-square residual than the event-based method; see the residuals in Figure 3.

5.3 Selkov and Fitzhugh Nagumo Oscillators. One of the particular strengths of our algorithm is that it inherently estimates the PRCs

Downloaded from http://direct.mit.edu/neco/article-pdf/37/12/2158/2554618/neco.a.32.pdf by Ramona Marchand on 07 December 2025

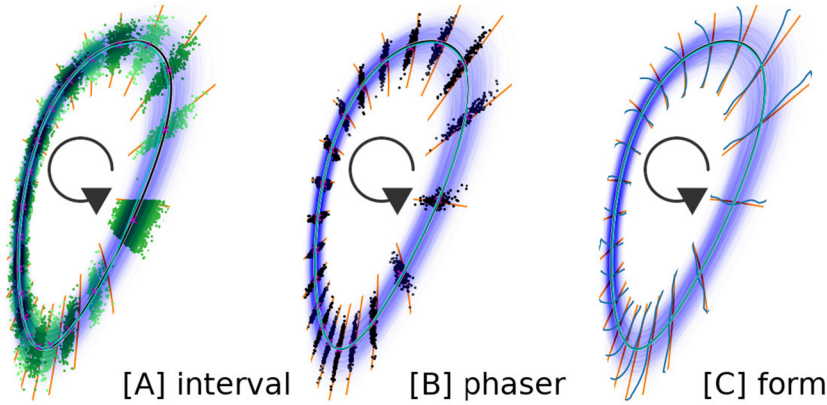


Figure 4: Comparison of stochastically driven Selkov oscillator isochrons obtained from the form-phase, and event-based phase estimates; the arrows indicate the direction of circulation. We plotted trajectories (blue), the limit cycle (true cycle—black, data-driven estimate—teal) and ground-truth isochrons from forward integration (orange lines). On top of those, we plotted scatter plots of trajectory points falling in 20 equally spaced intervals of width 0.02 period (A) green, alternating shades), Phaser (B) black; and form-based phase estimates (C) turquoise. Event phase estimates become noticeably poorer away from the event; Phaser estimates remain equally tight, but their angle to the limit cycle—the PRC—is incorrect; Form phase isochrons closely match the forward integration ground truth, that is, the angle between the thin lines in panel C are more acute than the angle between the black dots and orange lines in panel B.

(Ermentrout, 1996; Wilshin et al., 2021) of the system. We tested this capability with the stochastically perturbed Selkov oscillator (see Figure 4), and a stochastically perturbed version of the classical neuronal oscillator model—the FitzHugh-Nagumo (FitzHugh, 1961; Nagumo et al., 1962; Figure 5) system.

For Selkov, we took the two-dimensional system of the previous section and estimated the isochrons from three methods of phase estimation: event-based, taking phase to be the fraction of time between events; the Phaser algorithm (Revzen & Guckenheimer, 2008); and the form-phase based algorithm. We focused on the case of low system noise and highest initial condition noise, which corresponds closely with deterministic dynamics whose state space has been fully sampled. We found that event-based estimates of the ground-truth isochrons are poor, with a large spread in position and poor agreement with the ground truth. Phaser performed well on the limit cycle, but the angle of the limit cycle to the estimated isochrons was incorrect, indicating an erroneous PRC estimate. The form-phase estimate matched the deterministic isochrons far more closely. We

Downloaded from http://direct.mit.edu/neco/article-pdf/37/12/2158/2554618/neco.a.32.pdf by Ramona Marchand on 07 December 2025

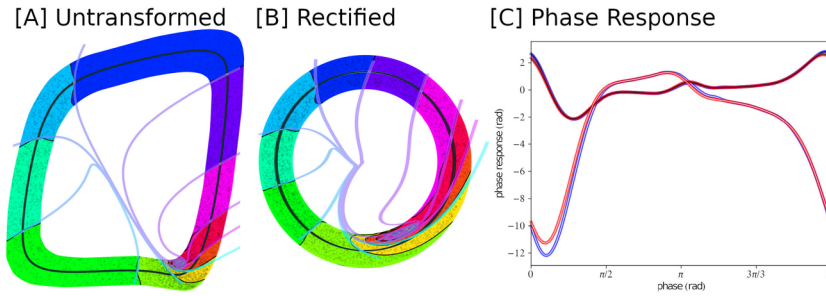


Figure 5: Temporal 1-Form based estimation of the FitzHugh-Nagumo oscillator isochrons (colored bands and solid black curves transverse to cycle). We uniformly sampled points within an annulus around the limit cycle in the rectified coordinates (6000 points, black dots). We then estimated the Temporal 1-Form with polynomial terms up to order 6, and Fourier terms of order up to 10. For comparison, we chose the same parameters as Figure 4 from Langfield et al. (2014) and overlaid their isochrons (pastel lines) on ours (black lines between colored regions). The results are shown in the original coordinates (A; limit cycle in black), and in rectified coordinates (B). The phase response curves (C) for this system as estimated by form phase (blue) and by forward numerical integration (in the sense used in Wilshin et al. (2021); red) for both x (white line interior) and y (black line interior) perturbations. Adapted from Langfield et al. (2014), with the permission of AIP Publishing.

conclude that form-phase-based phase estimates provided a superior estimate of the PRC.

Form-phase-based estimates can also easily be used for obtaining isochrons of systems for which the equations are known by using an importance sampling scheme. Figure 5 demonstrates this approach applied to the FitzHugh-Nagumo oscillator and compares our results with those of Langfield et al. (2015), which is a state-of-the-art method for systems with known equations of motion. FitzHugh-Nagumo is particularly challenging as it is a relaxation oscillator, which produces rapidly changing spikes with gaps of inactivity between them in a neuron-like spike train. Relaxation oscillators inherently have large changes in the magnitude of $d\phi$ on the limit cycle, exacerbating the effects of numerical errors on the estimation of isochrons. The results demonstrate that we can reproduce the isochrons next to the limit cycle and thus correctly reproduce the PRC for the FitzHugh-Nagumo oscillator when the complete state is available for measurement, or when the conditions of Wilshin et al. (2021) are met. This suggests we could reasonably expect our new algorithm to recover the PRC of neuronal oscillators when provided with sufficient data.

5.4 Phase Estimation from Partial Data in Guinea Fowl. Perhaps the most significant feature of our algorithm for its intended users is that our

Downloaded from http://direct.mit.edu/neco/article-pdf/37/12/2158/2554618/neco.a.32.pdf by Ramona Marchand on 07 December 2025

algorithm requires only state and state velocity pairs to calculate a phase estimate. It can be trained using short, disjointed training examples, even if no example contains more than a small portion of a cycle (see theorem 3 in section A.5). This is not true of any event-based phase, since the phase of all segments that do not contain the event cannot be determined at all. Similarly, Phaser cannot determine the phase of any data coming from a segment that does not cross the phase zero Poincaré section. Furthermore, because it uses the Hilbert transform to produce a protophase, Phaser requires each time series in its training data to be multiple cycles long; otherwise the Hilbert transform exhibits significant ringing artifacts.

We demonstrate the ability of our Temporal 1-Form algorithm to recover phase from short segments of data in Figure 6. Not only does it recover phase from input that only contains trajectory segments from partial cycles, the form phase also produces a similar result even when some of the data are omitted systematically from a large part of space. This data set with systematic omissions does not meet the requirements of our estimator convergence result (see theorem 3 in section A.5)—roughly speaking, it does not have a uniquely defined phase because a portion of the limit cycle is not observed—but it still seems to be usable, for reasons that remain to be understood (see remark 1 in section A.5).

5.5 Application to Chemical Oscillators. To illustrate how our algorithm could be applied to data from diverse sources, we obtained a sample of chemical oscillator data.[5] The raw measurements are seen in Figure 7 In these relaxation oscillators, the observable state is nearly constant away from their rapid "spike," and so it is difficult to extract useful state information far from these spikes. To provide a better numerically conditioned state, after renormalizing the oscillations to account for baseline drift and reagent depletion (see Figure 8 top), we passed the time series through a linear filter bank. We passed each signal through three Butterworth lowpass filters of order 2, with cutoffs computed from the median interspike interval (ISI) as half ISI, ISI, and twice ISI. We then used the difference of the first two as one set of lagged signals (see Figure 8 middle), and the difference of the last two as a second set of "lagged" signals (see Figure 8 bottom). These lagged signals have the property of being fairly sinusoidal, possessing phase responses close to $\pi/2$ apart and having very little response at DC (frequency 0). In short, they appear to provide a good augmented state space for the phase estimator to operate on (and it seems likely that this intuitive statement can be made mathematically rigorous using methods similar to those of Sauer et al., 1991). We then took the resulting phase estimates as real numbers, unwrapped them, and subtracted their time-dependent mean to obtain the relative phases (Revzen et al., 2008), showing clearly the convergence into two pairs of antiphase oscillators (see Figure 9).

[5] Our thanks for these data go to Seth Fraden and Michael Norton.

Downloaded from http://direct.mit.edu/neco/article-pdf/37/12/2158/2554618/neco.a.32.pdf by Ramona Marchand on 07 December 2025

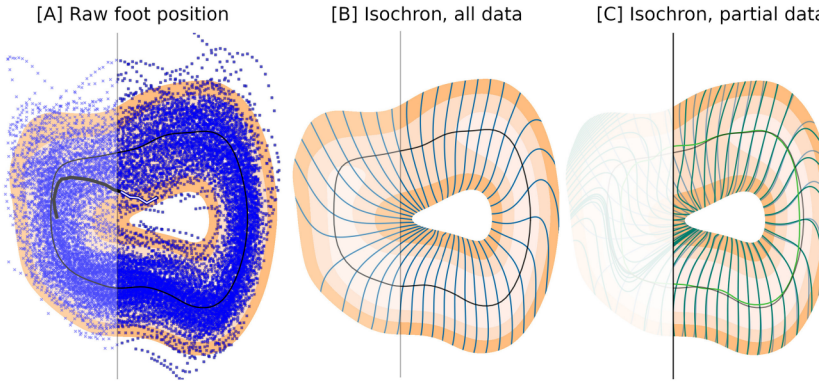


Figure 6: Estimating phase from partial data. Results for guinea fowl foot data, postprocessed adversely. We randomly split *Numida meleagris* foot motions (292 cycles; 250sps; running at 3Hz) into 20 sample segments with gaps > 40 samples in between. Segments were far shorter than cycles (A: blue dots all data; example segment wide solid green). We used the Temporal 1-Form phase estimator (order 6 Fourier, and order 6 polynomial terms), plotted the limit cycle estimate (order 10 Fourier model; B: solid black) and isochrons (B: light teal, every $\pi/20$ radians). We removed all data with $x < -0.5$ (arbitrary units; data are z-scored), about one-third of every cycle (A,B,C: vertical line; omitted data faded on left), and recomputed phase (order 6 Fourier terms; order 6 polynomial terms), and plotted the limit cycle C: solid green; same method) and the same isochrons (C: dark teal; full data isochrons faded light teal). We indicated amount of training data using a kernel smoothed density plot (50%, 70%, and 90% of maximum density; strong orange to pale orange). Even with fractional cycles and systematic inability to observe a large fraction of the cycle, most structure is recovered in both treatments wherever more than 70% of maximum data density is available. We remark that while accuracy of the isochron estimates in panel B is to be expected from theorem 3 (section A.5), it remains to be understood why reasonable accuracy is obtained in panel C (see the remark 1 in section A.5).

6 Conclusion

The definition of the Temporal 1-Form we provided shows that for smooth, exponentially stable oscillators, the phase obtained from the Temporal 1-Form agrees with the classical definition of asymptotic phase. Unlike the classical definition, the Temporal 1-Form makes evident (see section A.4) that asymptotic phase is in fact uniquely determined by a pointwise condition on forward the invariant sets.

This theoretical property allowed us to develop the presented algorithm and its performance guarantees (section A.5) for approximating the Temporal 1-Form of an oscillator from which a sample of noisy sample path

Downloaded from http://direct.mit.edu/neco/article-pdf/37/12/2158/2554618/neco.a.32.pdf by Ramona Marchand on 07 December 2025

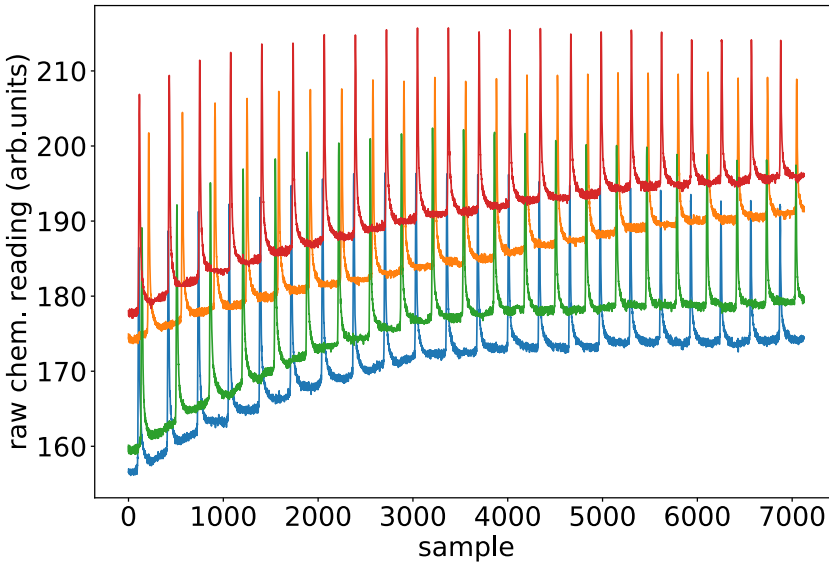


Figure 7: Raw data of optical transmission through four coupled cells running a Belousov-Zhabotinsky reaction; the four different colors (blue, red, green, cyan) show different cells undergoing the reaction. This is a chemical reaction where the opacity of a cell of varies as a complex, oscillatory chemical reaction occurs, the state of this reaction in a cell being coupled to the state of adjacent cells. Physical units are not provided because phase estimation does not require it.

segments is available. We have shown that this algorithm performs well on both simulated and experimental data. On simulated data of the Fitzhugh-Nagumo oscillator, a challenging relaxation oscillator system with known equations of motion, it performs comparably to the state-of-the-art algorithms that use those equations, even though our algorithm is entirely data driven and does not require the dynamics themselves to be integrated.

Our algorithm offers significant improvements over previously known methods for phase estimation:

1. Most important, the ability to estimate phase from state and state velocity pairs $(x, \dot{x})$ or, equivalently, pairs of consecutively sampled states (x_{n+1}, x_n). This capability in particular would make it attractive for modeling systems for which we are unable to obtain records of full periods of oscillation.
2. The ability to directly obtain PRCs from experimental time series data without knowledge of the equations of motion.

Downloaded from http://direct.mit.edu/neco/article-pdf/37/12/2158/2554618/neco.a.32.pdf by Ramona Marchand on 07 December 2025

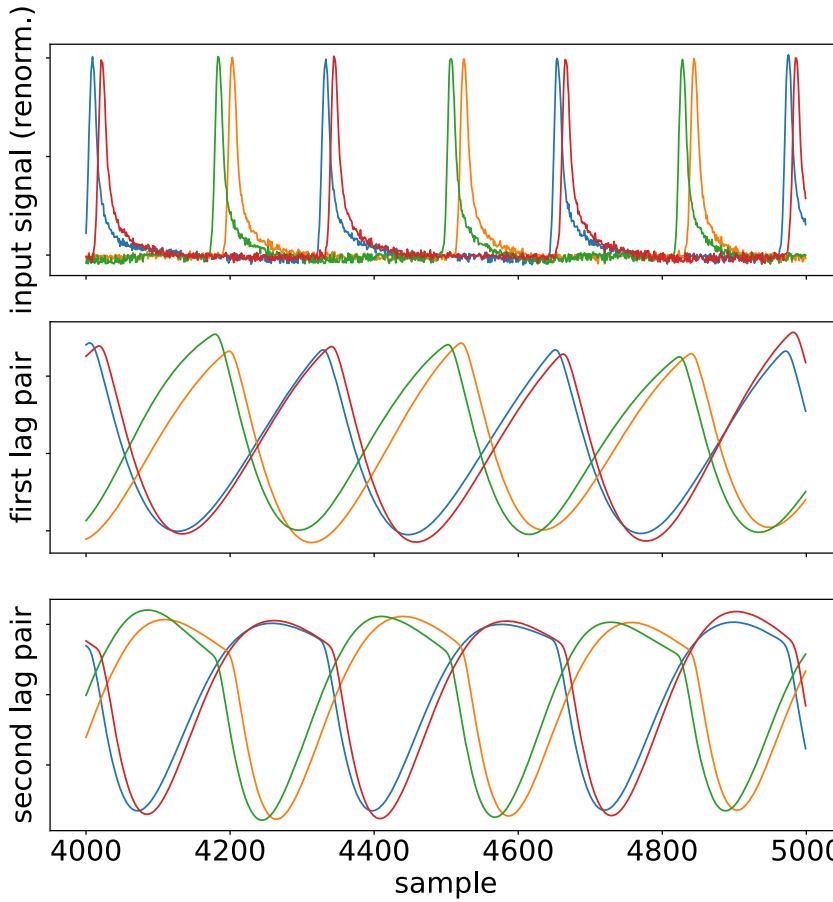


Figure 8: Data preparation of chemical oscillator data. These are the same data as in Figure 7, with the colors referring to the same oscillators, only (top) detrended and with a rescaled time series. We have computed the median interspike interval and filtered at 2 ISI (interspike interval) (here s1), 1 ISI (s2), and 0.5 ISI (s3). The middle panel shows the difference s1–s2 and the bottom the difference s2–s3.

3. More generally, the ability to estimate phase far from the limit cycle, in any forward invariant region containing enough data (see theorem 3 in section A.5).
4. Importantly, all of these abilities arise from an estimation procedure whose convergence we have proven and whose rates of convergence we have shown under reasonable assumptions about the measurement procedures (see section A.5). This implies that statistical power

Downloaded from http://direct.mit.edu/neco/article-pdf/37/12/2158/2554618/neco.a.32.pdf by Ramona Marchand on 07 December 2025

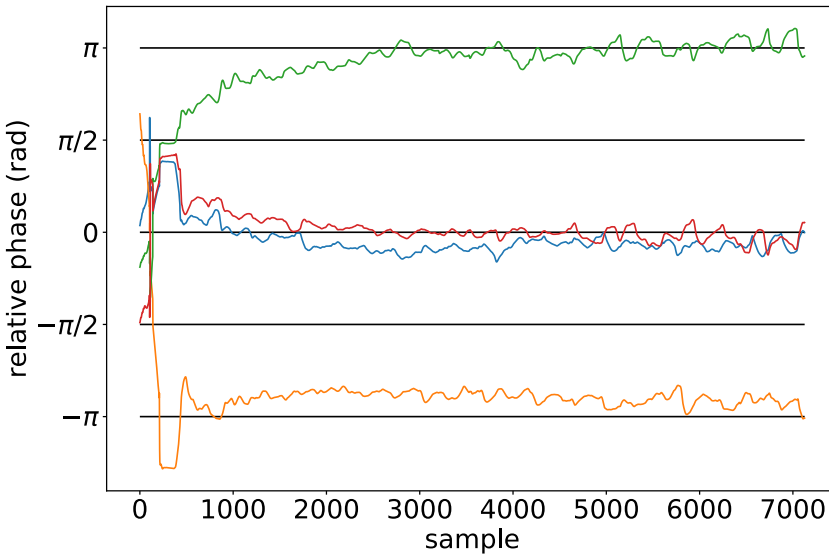


Figure 9: Relative phases of the oscillators in Figure 7, with colors again referring to the different cells, taken by training a phase estimator on the data, and subtracting the mean phase of all the oscillators.

calculations can be used to design experimental protocols that use our algorithm.

No other phase estimation method we are aware of possesses all of these useful properties.

In the years after our initial presentation of this method in 2014 (Wilshin & Revzen, 2014) and our 2017 publication (Wilshin et al., 2017), several groups have presented methods using a similar series expansion around a limit cycle as a means of reconstructing its Floquet structure. Some have been express about reconstructing the entire coordinate change given the eigenvalues (Pérez-Cervera & Huguet, 2020), and others (Wilson, 2020; Wilson & Ermentrout, 2018) started from focusing on phase and amplitude models and then provided additional modes later. These methods are similar to each other and are potentially quite valuable in reconstructing the dynamics of deterministic systems measured with noise. However, as originally noted in Revzen (2009) and Revzen and Guckenheimer (2012), even on carefully measured data sets, the numerically estimated return map eigenvalues change with the choice of Poincaré section (even if isochron sections are chosen). This is directly in contradiction to theory, which shows that monodromy matrices are related by a similarity transform, and therefore their eigenvalues should be identical. Other authors have also noted

Downloaded from http://direct.mit.edu/neco/article-pdf/37/12/2158/2554618/neco.a.32.pdf by Ramona Marchand on 07 December 2025

this (Wang & Srinivasan, 2012) and suggested the use of multiple sections simultaneously as a means for improving the estimation procedure. For fluid dynamics problems, which possess a great many local symmetries, the use of DMD and related algorithms (Kutz et al., 2016) has led to some success in obtaining robust eigenvalue estimates in addition to the unit circle "phase" eigenvalue and the slowest decaying "isostable" mode, but often these modes are part of the parabolic family of eigenvalues that arise from harmonics of the slowest mode due to the quality factor of the oscillator (Bagheri, 2014)—that is, they are expressions of the phase diffusion of the isostable rather than expressions of other Floquet modes. While new DMD variants are continuously being added, most of the approaches listed in even the most recent reviews of DMD (Colbrook, 2024) have not been demonstrated to work on the locomotion data that motivate our work. As it stands, it is doubtful the methods that rely on eigenvalues as a starting point could correctly estimate the structure of the coordinate change when those eigenvalues are themselves not reliably known.

Because the Temporal 1-Form can be estimated from short time series segments, it offers the opportunity to study a broad range of oscillatory phenomena that were previously hard to analyze—because of either prohibitively long oscillation period or technical difficulties in obtaining multiperiod measurements. We have shown that a Temporal 1-Form estimator can be successfully trained on short fragments of cycles, and will still estimate the isochrons accurately and consistently (e.g., the oscillator associated with the guinea fowl feet). Event-based methods such as anterior extreme position detection (Cruse & Schwarze, 1988) or heel-strike (Ting et al., 1994; Jindrich & Full, 2002) detection cannot use such fragmented data as the decisive event need not appear in every fragment of data. The Phaser algorithm cannot solve this problem either, as it performs a Hilbert transform to calculate its initial proto-phases, introducing transients on the order of one to three cycles.

The Temporal 1-Form allows one to detect the phase response to perturbations of the underlying deterministic dynamics. The phase response describes only the effect of perturbation that persists after a long time, and even the infinitesimal phase response approximation—the PRC—allows the observed system to be modeled in the weakly coupled oscillator approximation. This PRC is available directly from the Temporal 1-Form phase estimation procedure, paving the way to empirically generated oscillator coupling models in many domains.

For scientists studying oscillatory systems, a phase-based model allows the experimentalist to compare the outcome of experimental treatment (e.g., a mechanical perturbation to locomotion) to that of the counterfactual unperturbed system modeled as a deterministic function of phase (Revzen et al., 2008). The results in section 5.2 indicate that for systems of different dimensions, levels of diffusion, and initial condition noise, approximating phase using a Temporal 1-Form produced by the algorithm presented here

Downloaded from http://direct.mit.edu/neco/article-pdf/37/12/2158/2554618/neco.a.32.pdf by Ramona Marchand on 07 December 2025

is superior to event-based phase estimates commonly used in the experimental literature and to the Phaser algorithm. In the examples we studied, the mean-square error of the phase estimate from the form-based technique is smaller. The inferred isochrons are closer to the ground truth, and the PRC-s are more accurate.

The work of Rafiee, Shakiba, and Kiemel (Rafiee & Kiemel, 2020), although limited to finding the PRC or ϕIRF, brought up the question of phase estimation without a complete state measurement. Our method addresses this issue at least in part, because in a formal sense, all unmodeled dynamics are forms of system noise. To the extent that ensembles of observed states posess a convergent second moment, our proof that the Temporal 1-Form estimate converges to the "correct" Temporal 1-Form remains true. However, which notion of phase is the correct one to apply when different types of system noise exist is itself a matter of active debate in the literature. In this sense, we offer a contender: the maximum likelihood estimate of the Temporal 1-Form given the underlying distribution of initial states (observed or unobserved) is an answer that we have shown to be consistent with the deterministic definition of phase when the dynamics are deterministic. Unlike the methods of Rafiee and Kiemel (2020), it extends beyond the infinitesimal neighborhood of the limit cycle and provides an estimate of the phase difference between states averaged on the training data ensemble.

Because of the very weak assumptions required in section A.5.1 for our convergence proofs, theorems 2 and 3, we expect the method we presented is of very broad applicability. One limitation of our approach is seen in remark 4: the larger the norm of the Temporal 1-Form, the harder it is for the estimate to converge. This implies that for very stiff relaxation oscillators, the Temporal 1-Form estimate will converge more slowly. If some regions converge to the limit cycle quickly and other regions converge slowly, the data available from any practical experiment will be highly undersampled in the fast regions compared with the slow regions, leading to a Temporal 1-Form in the fast regions that is dominated by the extrapolated data from the slow regions. In such cases, depending on application, it might be good to impose a resampling scheme to make the data density more uniform. The convergence rate of our algorithm is tied to the convergence rate of the first and second moments of the underlying noise. If the system has, for example, a heavy-tailed measurement outlier process, this could significantly affect convergence rates, as it would any statistical moments. Finally, our choice to use the monomial basis for the radial part of our basis functions is simple but less sample efficient than picking an orthogonal family of polynomials.

Future work may extend our algorithm by application of domain-specific knowledge, in particular by incorporating new basis forms and coordinate change methods. Such extensions would certainly speed up the algorithm and improve its accuracy. It is possible that with large data sets or by using a pretrained "foundation model" trained on large corpori from

Downloaded from http://direct.mit.edu/neco/article-pdf/37/12/2158/2554618/neco.a.32.pdf by Ramona Marchand on 07 December 2025

the domain of interest, the residual dynamics around the limit cycle could also be modeled with conventional machine learning approaches. However, removing the topological obstruction to such models by subtracting a suitable circulation produces a decisive advantage that we expect to extend to any data-driven function-fitting framework.

The Temporal 1-Form offers a new perspective on the notion of phase in nonlinear oscillators, as well as a new way to obtain oscillator and PRC models from experimental data.

Appendix A: Data Preparation and Properties of the Temporal 1-Form

This appendix is written with mathematically inclined readers in mind. As such, we presume familiarity with fundamental concepts of differential topology (Guillemin & Pollack, 2010; Hirsch, 1976; Lee, 2013), differential forms (Spivak, 1971; Guillemin & Pollack, 2010; Lee, 2013), and stochastic differential equations (Arnold, 1974; Gardiner, 2004; Evans, 2013; Øksendal, 2013).

A.1 Generating Ground Truth Test Data—Details. This section provides details of the method we used to generate randomized test systems with adjustible complexity and noise characteristics. We provide these details, and the related code, in the hope that other investigators may use them to evaluate the performance of algorithms that aim to analyze the structure of nonlinear oscillators.

Very few oscillators admit a closed-form representation of their phase as a function of state, which made the validation of our algorithm a significant challenge all on its own. To produce a well-specified class of tests for our algorithm, we produced sample paths arising from a Stratonovich stochastic differential equation of the form

$$\mathrm{d}x(t) = f(x(t))\mathrm{d}t + G(x(t)) \circ \mathrm{d}W(t), \tag{A.1}$$

while requiring that the deterministic dynamics of $\mathrm{d}x(t) = f(x(t))\mathrm{d}t$ are known to be a (hyperbolic) limit cycle oscillator, with a known phase coordinate.

We obtained such a deterministic oscillator by starting with a randomly chosen linearized (Floquet) structure converging on the trajectory $x(t) = [t, 0, \ldots]$, then winding this affine system around the unit circle with x_1 as the angle, and finally pushing forward the dynamics through a composition of randomly generated diffeomorphisms to generate $f(\cdot)$ of equation A.1. We chose diffeomorphisms such that their tangent maps were computable and invertible in closed form. We used a second composition of random diffeomorphisms to generate a function $g(\cdot)$, and the inverse of the tangent map of $g(\cdot)$ was used for $G(\cdot)$. By using the inverse diffeomorphisms, we

Downloaded from http://direct.mit.edu/neco/article-pdf/37/12/2158/2554618/neco.a.32.pdf by Ramona Marchand on 07 December 2025

directly computed the phase of each trajectory point with respect to the deterministic dynamics to use as a baseline for comparing with other forms of phase estimation.

A.1.1 Implementation of the Floquet Structure. While our exposition so far has focused on differential forms, allowing us to emphasize the coordinate-invariant properties of the Temporal 1-Form, we provide the equations in this section in a computationally friendly coordinate dependent matrix notation.

Given an n-dimensional state space ($n > 1$), we defined a vector field by first taking the polar decomposition $\Omega : \mathbb{R}^n \to S^1 \times \mathbb{R}^+ \times \mathbb{R}^{n-2}$ of the first two coordinates: $p := [x_3, x_4, \ldots]$, $\theta := \text{atan2}(x_1, x_2)$, $r := \sqrt{x_1^2 + x_2^2}$ and thus $\Omega(x) = [\theta, r] \oplus p$.

In these polar coordinates, the equation of motion we implemented is affine:

$$\begin{aligned} \dot{\theta} &= 1, \\ \dot{r} &= \beta(r-1) + c_r^{\mathsf{T}} p, \\ \dot{p} &= \gamma(r-1) + Mp. \end{aligned} \tag{A.2}$$

This means that $\dot{\theta}$ is, for a deterministic system, uniformly advancing in time, and the latter two equations comprise an autonomous linear subsystem that evolves independent of θ. These equations can be combined to form a single equation in homogeneous coordinates:

$$[\dot{\theta}, \dot{r}, \dot{p}, 0]^{\mathsf{T}} = \tilde{M}[\theta, r, p, 1]^{\mathsf{T}}, \tag{A.3}$$

where the matrix $\tilde{M}$ can be chosen to obtain any eigenvalue structure desired for the dynamics.

A.1.2 A Natural Class of Invertible Diffeomorphisms. To produce randomized invertible diffeomorphisms, we used a structure inspired by the Hénon map (Hénon, 1976) (and therefore refer to these as H-maps) and recommended to us by J. M. Guckenheimer. Given: A (split) vector space $\mathbf{Q} := \mathbf{U} \oplus \mathbf{V}$; invertible maps $g_U : \mathbf{U} \to \mathbf{U}$ and $g_V : \mathbf{V} \to \mathbf{V}$; and a (possibly non-invertible) map $f : \mathbf{V} \to \mathbf{U}$, we constructed the following mapping:

$$\tilde{x} := g_U(x) + (f \circ g_V)(y) \qquad \tilde{y} := g_V(y), \tag{A.4}$$

which admits the inverse (by construction):

$$x := g_U^{-1}(\tilde{x} - f(\tilde{y})) \qquad y := g_V^{-1}(\tilde{y}). \tag{A.5}$$

Downloaded from http://direct.mit.edu/neco/article-pdf/37/12/2158/2554618/neco.a.32.pdf by Ramona Marchand on 07 December 2025

In our implementation, we have chosen to make g_U and g_V affine maps. For our nonlinear map $f(\cdot)$, we used inversions of the form

$$f(x) := m(\beta + 2)\frac{\varrho(x)P(x)}{\left(\varrho(x)^2 + \beta\varrho(x) + 1\right)}, \tag{A.6}$$

$$\varrho(x) := \left(x^{\mathsf{T}}Ax\right), \tag{A.7}$$

for some positive symmetric A with eigenvalues close to one (uniformly randomly sampled between 0.95 and 1.05 for our simulations). f is a function that is approximately zero when $\varrho(x)$ is small and large and is stationary with value m at $\varrho(x) = 1$. It has one stationary point for positive values of $\varrho(x)$ with β controlling how peaked the function is (the more negative beta is, the greater the peaking). P maps from $\mathbf{U}$ of dimension D_U to $\mathbf{V}$ of dimension D_V and the components of P are given by.

$$P_{ij} = \begin{cases} 1 & \text{if } i \equiv j \,[\text{mod } D_U] \\ 0 & \text{if } i \not\equiv j \,[\text{mod } D_U], \end{cases} \tag{A.8}$$

with $1 \leq i \leq D_V$ and $1 \leq j \leq D_U$.

We composed together a sequence of these maps to produce a highly nonlinear, but invertible, distortion of the Floquet system after it has been transformed to polar coordinates. Between each pair of consecutive H-maps, we inserted a randomly chosen full-rank affine transformation.

A.1.3 Stochastic Integration of the Combined System. We implemented individual diffeomorphisms as objects of a `Python` class using the SciPy scientific programming environment. Each mapping object was capable of forward and inverse mappings, push-forwards and pullbacks. We composed these mapping objects with each other to construct the fully formed random diffeomorphisms for both the deterministic and noise terms of equation A.1. The noise term uses the Jacobian of an H-map chain to transform the Wiener process when integrating the SDE. The final integrated Floquet system is then transformed by a different H-map chain. We integrated the SDE of equation A.1 using an implementation of the R3 stochastic integration scheme (Bastani & Hosseini, 2007; Burrage, 1999), and have made this integrator available publicly as part of the form phase package. We also note that while the ground-truth isochrons of the deterministic system are known precisely, they may not be compatible with various ground-truth definitions of stochastic isochrons (Schwabedal & Pikovsky, 2013; Thomas & Lindner, 2014; Cao et al., 2020; Engel & Kuehn, 2021) for the SDE. For example, the presence of noise can change the average frequency of a limit cycle oscillator and, by extension, may deform the isochrons. We expect that while at the low noise limit our recovered

Downloaded from http://direct.mit.edu/neco/article-pdf/37/12/2158/2554618/neco.a.32.pdf by Ramona Marchand on 07 December 2025

phase will closely match the deterministic system (this expectation is mathematically justified in section A.5.2), as noise is increased, the discrepancy between the two may justifiably increase. We therefore caution that in the presence of consistent systematic errors and higher noise conditions, errors in estimates of asymptotic phase may represent an error in the ground truth rather than an estimation error on the part of the algorithm.

A.1.4 The Noise Terms. Our system uses three different sources of noise. The first is the variation in the initial conditions and is not used during integration. The initial conditions are chosen in the untransformed space whose evolution is specified by equation A.2. The phase coordinate is simply uniformly randomly sampled (from 0 to 2π in radians). For the remaining coordinates, a sample from uniform random distribution from $-\eta_{init}/2$ to $\eta_{init}/2$ is added to the value of these coordinates on the limit cycle (the limit cycle has these coordinates constant). For our test systems, the value of η_{init} are given in the first column of Table 2.

The diffusion term (the last term of equation A.1) has a block diagonal structure, with a separate magnitude for the noise of the phase term (the first coordinate, θ), and the remaining coordinates. For the noise term G in equation A.1 is the identity transform and the magnitude of the wiener term is given in the third column of Table 2. For all coordinates, the magnitude of the wiener term is set to the second column of Table 2 and transformed as described in the previous section.

A.1.5 Preparation of Data for Phase Estimation. In each simulation, we treated these D-dimensional data similarly to how experimental data would be treated. We filtered the data using a Kalman smoother (Briers et al., 2009) with the system states the position and its derivative. The state transition matrix assumed no acceleration and that the last D coordinates were derivatives of the first D coordinates. The observation matrix was a $D \times 2D$ matrix with an identity in the first $D \times D$ submatrix. We assumed the system noise matrix to be diagonal with the first D system variables having the same level of variance and the last D variables having a (typically) different shared level variance. We estimated these two system covariance parameters by maximizing the likelihood of the training observations.

After filtering, we performed a principal component analysis and rotated the system into the corresponding orthogonal coordinate system. We then z-scored the first two principal components.

A.2 Review of Differential Forms. Differential forms Ω over a manifold $\mathbf{M}$ are an exterior algebra generated using two operators: the exterior product $\wedge$—the universal skew symmetric product—and the exterior derivative $\mathbf{d}$. Elements of rank 0 correspond to (sufficiently smooth) scalar valued functions $\mathbf{M} \to \mathbb{C}$. When $\alpha \in \Omega_r$ and $\beta \in \Omega_s$, $\mathbf{d}\alpha \in \Omega_{r+1}$ and $\alpha \wedge \beta \in \Omega_{r+s}$.

Downloaded from http://direct.mit.edu/neco/article-pdf/37/12/2158/2554618/neco.a.32.pdf by Ramona Marchand on 07 December 2025

These operations are familiar to many in their three-dimensional special cases, where ranks $\Omega_0, \ldots, \Omega_3$ correspond to scalar functions, vectors, directed areas, and directed volumes. In 3D, the exterior derivative $\mathbf{d}$ functions as the gradient, curl, and divergence. The exterior product $\wedge$ functions as a scalar-vector product when one argument is rank 0 as a cross product (resulting in a directed area) when the arguments are rank 1 and as a box product when applied to rank 2 and rank 1 arguments.

Formally defined, $\mathcal{C}^k$ differential 1-forms α on $\mathbf{M}$ are $\mathcal{C}^k$ sections of its cotangent bundle $\mathsf{T}^*\mathbf{M}$: $\alpha(x) \in \mathsf{T}^*_x\mathbf{M}$. If v is a $\mathcal{C}^k$ vector field, then $\langle \alpha, v \rangle$ is a $\mathcal{C}^k$ scalar function. If α is a $\mathcal{C}^1$ curve in $\mathbf{M}$, the line integral $\int_\alpha \alpha$ is well defined and independent of coordinate system.

A 1-form α is closed if its exterior derivative vanishes. It is exact if it is the exterior derivative of a scalar function. The identity $\mathbf{d} \circ \mathbf{d} = 0$ implies that all exact forms are closed. On contractible regions of $\mathbf{M}$, the converse is true, that is, all closed forms are exact (a.k.a. the Poincaré lemma). The quotient space of closed to exact k-forms is known as the kth de Rham cohomology group. We use some properties of this cohomology to construct our algorithm.

If a closed curve γ_1 can be smoothly deformed into a curve γ_2, $\int_{\gamma_1} \alpha$ of a closed 1-form α equals $\int_{\gamma_2} \alpha$. In other words, the integral of a closed 1-form depends only on the homotopy class of the underlying closed curve.

A fuller introduction to the theory of differential forms can be found in Spivak (1971), Guillemin and Pollack (2010), and Lee (2013).

A.3 Temporal 1-Form. This self-contained section which serves as an alternative introduction to our article, which contains more details and is aimed at more mathematically inclined readers. It includes a description of the Temporal 1-Form assuming some familiarity with differential forms, which are reviewed in section A.2.

We consider continuous-time dynamical systems, or flows Φ, on a smooth n-dimensional manifold $\mathbf{M}$. That Φ is a flow means that $\Phi : \mathbf{M} \times \mathbb{R} \to \mathbf{M}$, $\Phi_0 = \mathrm{id}_\mathbf{M}$, and $\Phi_t \circ \Phi_s = \Phi_{t+s}$. We assume that the vector field $f := \frac{\partial}{\partial t} \Phi_t|_{t=0}$ is well defined and $\mathcal{C}^{k \geq 1}$, so that $\Phi \in \mathcal{C}^k$. The trajectories $t \mapsto \Phi_t(x_0) =: x(t)$ satisfy the ordinary differential equation (ODE) $\dot{x} = f(x)$. A periodic orbit o of period $T > 0$ is a trajectory that satisfies $o(t + T) = o(t)$ with $o(t) \neq o(0)$ for all $0 < t < T$. We will always assume that $T > 0$ is the minimal period of a nonstationary periodic orbit. We focus on dynamical systems possessing only one nonstationary periodic trajectory o and denote by $\Gamma \subset \mathbf{M}$ the image of this o.

We further assume that this periodic trajectory is exponentially stable, a property that holds in many practical cases. Exponentially stable limit cycles are always "normally hyperbolic" (Hirsch et al., 1977; Eldering et al., 2018); for brevity we simply refer to these as limit cycles. We refer to the stability basin of a limit cycle and the dynamics within it as an oscillator. The

Downloaded from http://direct.mit.edu/neco/article-pdf/37/12/2158/2554618/neco.a.32.pdf by Ramona Marchand on 07 December 2025

asymptotic behavior of any oscillator is described fully by its asymptotic phase: the stability basin of an oscillator is partitioned into codimension-1 $\mathcal{C}^k$ embedded submanifolds (Eldering et al., 2018) called "isochrons" which are asymptotically in phase with one another (Guckenheimer, 1975; Winfree, 1980).

For systems in which the dimension is low, the noise is small, or the data are plentiful, data pairs $(x_k, \dot{x}_k)$, $k = 1, \ldots, N$ may be used to estimate the vector field f. Numerous investigators proposed such approaches, primarily in the 1990s. Classical papers include Kostelich and Yorke (1990), who fit arbitrary continuous dynamics to trajectories, and the rich literature on time-delay embeddings, derivatives, and principal components (Takens, 1981; Sauer et al., 1991; Schelter et al., 2006; Gibson et al., 1992). When dynamical equations are known precisely, automatic differentiation and continuation methods can be used to compute the isochrons, a problem equivalent to that of phase estimation (Huguet & de la Llave, 2012; Osinga & Moehlis, 2010). However, care must be taken if it is desired to extract PRC from this, as these quantities are coordinate dependent projections of the Temporal 1-Form (Wilshin et al., 2021).

With fewer data points and higher levels of noise, one expects that the full off-cycle dynamics are less amenable to accurate estimation and that only a few of the slower-decaying modes might be observable off the limit cycle (Revzen & Guckenheimer, 2012). At the extreme, only phase itself might be detectable, through methods such as we proposed in Revzen and Guckenheimer (2008) using various phase-locking approaches (Peters & Schaal, 2008; Schaal & Atkeson, 2010; Schaal et al., 2005). This motivates the main goal of this article: estimate asymptotic phase from empirically observed dynamics, for example, from an ensemble of noisy measurements of (possibly short and noisy) system trajectory segments.

We note that, while there has been work to define generalized notions of asymptotic phase for stochastic oscillators (Schwabedal & Pikovsky, 2013; Thomas & Lindner, 2014; Cao et al., 2020; Engel & Kuehn, 2021 also see (Pikovsky, 2015, and Thomas & Lindner, 2015) for a spirited discussion), in this article we restrict ourselves to estimation of the classical asymptotic phase of a deterministic oscillator using data from a perturbed version of the underlying deterministic system. We also note that there are operator-theoretic methods of recent interest revealing phase as the generator of a family of eigenfunctions of the Koopman operator with purely imaginary eigenvalues (Mauroy & Mezić, 2012; Kvalheim & Revzen, 2021; Kvalheim, Hong et al., 2021). These eigenfunctions and others can be estimated using Fourier/Laplace averages (Mauroy & Mezić, 2012; Mauroy, Mezić et al., 2013; Kvalheim & Revzen, 2021; Kvalheim, Wong et al., 2021; Brunton et al., 2021) when dynamical equations are known and from data using dynamic mode decomposition (Kutz et al., 2016), at least in certain cases. However, the results of these emerging spectral methods seem to be very sensitive to the choice of observables and their nonlinearities (Wu et al., 2021).

Downloaded from http://direct.mit.edu/neco/article-pdf/37/12/2158/2554618/neco.a.32.pdf by Ramona Marchand on 07 December 2025

Several investigators have pursued the construction of linearized (Floquet) models for dynamics near the limit cycle. We proposed an approach termed "data driven Floquet analysis" (DDFA) (Revzen et al., 2011; Revzen, 2009) consisting of an estimating phase, then constructing affine models conditioned on phase. Tytell (2013) reported a DDFA approach based on harmonic balance. Wang and Srinivasan (2012) proposed to construct a Floquet model using factored Poincaré maps and derive a phase estimate from this model. Ankarali and Cowan (2014) applied "harmonic transfer functions" and achieved good results on a hybrid (Back et al., 1993; Simić et al., 2000; Westervelt et al., 2003; Ames & Sastry, 2005; Goebel et al., 2009; Lerman, 2016; Lerman & Schmidt, 2020; Clark & Bloch, 2021; Kvalheim, Gustafson et al., 2021) spring-mass hopper model. Regardless of how they are obtained, linear models of the dynamics around the limit cycle can at best only represent the hyperplanes tangent to the isochrons at their intersection with the limit cycle. By contrast, the method we propose here can construct nonlinear isochron approximations on suitable neighborhoods of the limit cycle, as we explain in section A.5.

We now begin our theoretical description of the Temporal 1-Form. By redefining $\mathbf{M}$ to be the basin of attraction of Γ, we henceforth assume that Γ is globally asymptotically stable. Asymptotic phase can be viewed as a map $\mathrm{P} : \mathbf{M} \to \Gamma$, which is a retraction ($\mathrm{P}|_\Gamma = \mathrm{id}|_\Gamma$) and a semiconjugacy ($\forall t \in \mathbb{R} : \mathrm{P} \circ \Phi_t = \Phi_t \circ \mathrm{P}$). From this it follows that $\mathrm{P} \in \mathcal{C}^k$ when $f \in \mathcal{C}^k$.[6] Each $p \in \Gamma$ represents the "isochron" $\mathrm{P}^{-1}(p)$, which is the set of initial conditions from which trajectories converge with the one starting at p.[7] In the context of oscillators, asymptotic phase is more commonly represented as a circle-valued ("phasor"-valued) map $\varphi : \mathbf{M} \to \mathrm{S}^1$; we explain the relationships of different representations of phase in section A.4.

The Temporal 1-Form appears naturally as a consequence of the existence of P. Noting that f is nowhere zero on the one-dimensional $\mathcal{C}^k$ manifold Γ and defining the angular frequency $\omega =: 2\pi/T$, it follows that there exists a unique $\mathcal{C}^{k-1}$ differential 1-form α on Γ satisfying $\langle \alpha, f \rangle = \omega$ identically on Γ.[8] The Temporal 1-Form $d\phi : \mathbf{M} \to \mathsf{T}^*\mathbf{M}$ is defined to be the pullback $\mathrm{P}^*\alpha$ of α, which means that $\langle d\phi(x), v \rangle := \langle \alpha(\mathrm{P}(x)), \mathsf{D}\mathrm{P}(x) \cdot v \rangle$ for any $v \in \mathsf{T}_x\mathbf{M}$. Since $\mathrm{P} \in \mathcal{C}^k$, it follows that $d\phi \in \mathcal{C}^{k-1}$. It is easy to see that the

[6] In more detail: fix $x \in \mathbf{M}$, let $U \subsetneq \Gamma$ be a contractible open neighborhood of $\mathrm{P}(x)$, and define $\tau_x \in [0, \infty)$ to be the smallest nonnegative number such that $\mathrm{P} \circ \Phi_{-\tau_x}(x) = o(0)$. Since the isochron $\mathrm{P}^{-1}(o(0))$ is a $\mathcal{C}^{k \geq 1}$ manifold transverse to the vector field (Guckenheimer, 1975; Eldering et al., 2018), the implicit function theorem implies that there is a $\mathcal{C}^k$ function $\tau : \mathrm{P}^{-1}(U) \to \mathbb{R}$ satisfying $\tau(x) = \tau_x$ and $\mathrm{P} \circ \Phi_{-\tau(y)}(y) = o(0)$ for all $y \in \mathrm{P}^{-1}(U)$. Thus, $\mathrm{P}|_{\mathrm{P}^{-1}(U)} = o \circ \tau$ is $\mathcal{C}^k$. Since $x \in \mathbf{M}$ was arbitrary, it follows that $\mathrm{P} \in \mathcal{C}^k$.

[7] The geometry of isochrons can be surprisingly complicated, especially when the vector field f has multiple timescales (Langfield et al., 2015).

[8] In a Euclidean space, α can be expressed as $\alpha := (f^\mathsf{T} f)^{-1} \omega f^\mathsf{T}$.

Downloaded from http://direct.mit.edu/neco/article-pdf/37/12/2158/2554618/neco.a.32.pdf by Ramona Marchand on 07 December 2025

Temporal 1-Form satisfies two properties (further discussed in section A.4): (1) $\langle d\phi, f\rangle = \omega$ everywhere, and (2) $d\phi$ is closed.

By "closed" we mean that each $x \in \mathbf{M}$ possesses an open neighborhood U_x on which $d\phi$ is the exterior derivative of a $\mathcal{C}^k$ function. This definition permits us to discuss continuous closed forms, needed for the case $f \in \mathcal{C}^1$; it reduces to the usual definition for $\mathcal{C}^1$ forms (Farber et al., 2004).

Somewhat less obvious is the fact that the Temporal 1-Form is the unique continuous closed 1-form on $\mathbf{M}$ satisfying the preceding two properties; we show that this is the case in section A.4. In that section we also relate P, $d\phi$, and circle-valued phases $\varphi : \mathbf{M} \to \mathrm{S}^1$. By a "circle-valued (asymptotic) phase" $\varphi : \mathbf{M} \to \mathrm{S}^1 \subset \mathbb{C}$, we mean a continuous map satisfying $\varphi \circ \Phi_t = e^{i\omega t}\varphi$ for all $t \in \mathbb{R}$. To summarize theorem 1 of section A.4, some of these relationships are as follows: $\varphi \circ \mathrm{P} = \varphi$, φ is unique modulo rotations of S^1, and $d\phi = \varphi^*(d\theta)$ is the pullback of the standard angular form on S^1 via any circle-valued phase. Moreover, any choice of base point $x_0 \in \mathbf{M}$ uniquely determines a circle-valued phase by integrating $d\phi$ along continuous curves from x_0.

While we are interested in asymptotic phase as defined for deterministic oscillators, our primary goal is to compute asymptotic phase from real-world data, which we assume may be subject to system and measurement noise. In section A.5, we derive fairly general performance guarantees applicable to our algorithm and potentially others. In that section, we define "unobserved" and "observed" empirical cost functions J_N and $\widehat{J_N}$ mapping 1-forms to nonnegative numbers, where N is the number of observed state-velocity data pairs. Intuitively, we would like to minimize the former cost (for which $J_N(d\phi) = 0$), but only the latter cost is observable, so our algorithms attempt to minimize the latter.

We assume that our algorithm outputs estimates $\widehat{d\phi}_N$ satisfying $\|\widehat{d\phi}_N - d\phi\|_{\mathcal{C}^0(K)} \leq \epsilon$ for some $\epsilon \geq 0$ (where $\|\cdot\|_{\mathcal{C}^0(K)}$ denotes the supremum norm), that $\mathbf{M}$ is an open subset of $\mathbb{R}^n$, and that state measurements belong to some fixed compact set $K \subset \mathbf{M}$. We establish in theorem 2 the following inequality holding with probability 1:

$$\limsup_{N\to\infty} \frac{\sqrt{J_N(\widehat{d\phi}_N)} - 2\sqrt{\epsilon}}{\|d\phi\|_{\mathcal{C}^0(K)} + (1+\sqrt{2})\|\widehat{d\phi}_N\|_{\mathcal{C}^0(K)}} \overset{\text{a.s.}}{\leq} 2\sqrt{\kappa}.$$

Assuming $\epsilon = 0$ for simplicity, it follows in particular that with f fixed, the performance of the estimator with respect to J_N is within $\mathcal{O}(\kappa)$ of optimality in the limit of large data. Moreover, the full statement of theorem 2 also includes explicit convergence rates (see remark 3). See the remarks following theorem 2 for further discussion.

However, as discussed in section A.5, bounding the performance with respect to J_N as in theorem 2 does not say anything about the closeness of the estimates $\widehat{d\phi}_N$ themselves to $d\phi$. Thus, even if $J_N(\widehat{d\phi}_N)$ is small, the estimated

Downloaded from http://direct.mit.edu/neco/article-pdf/37/12/2158/2554618/neco.a.32.pdf by Ramona Marchand on 07 December 2025

isochrons corresponding to $\widehat{d\phi}_N$ need not resemble the true isochrons. This motivates theorem 3, which shows, roughly speaking, that under some additional assumptions, the estimated isochrons converge $\mathcal{C}^1$-uniformly to the true isochrons on forward invariant open subsets of K. Moreover, the full statement of theorem 1 also includes explicit convergence rates.

A.4 Relationship of the Temporal 1-Form to Other Representations of Asymptotic Phase. In this section, we explain the relationship (mentioned in section A.3) of the asymptotic phase map $\mathrm{P} : \mathbf{M} \to \Gamma$, circle-valued phase maps $\varphi : \mathbf{M} \to \mathrm{S}^1$, and the Temporal 1-Form $d\phi$. We continue under the assumptions and notation of section A.3; in particular, the state space $\mathbf{M}$ is also the basin of Γ.

Lemma 1. *Consider an oscillator generated by the $\mathcal{C}^1$ vector field $f : \mathbf{M} \to \mathsf{T}\mathbf{M}$. The Temporal 1-Form $d\phi : \mathbf{M} \to \mathsf{T}^*\mathbf{M}$ is closed and satisfies $\langle d\phi, f\rangle \equiv \omega$.*

Proof. Since $\mathrm{P} : \mathbf{M} \to \Gamma$ is a semiconjugacy, it follows that $\mathsf{D}\mathrm{P} \circ f = f \circ \mathrm{P}$. Since $d\phi =: \mathrm{P}^*\alpha$ (see section A.3), it follows that $\langle d\phi, f\rangle \equiv \langle P^*\alpha, f\rangle \equiv \langle \alpha, \mathsf{D}P \circ f\rangle \equiv \langle \alpha, f \circ P\rangle \equiv \omega$. Since α is closed and pullbacks commute with $\mathbf{d}$, $d\phi = \mathrm{P}^*\alpha$ is closed. □

Given an open neighborhood $U \subset \mathbf{M}$ of Γ, which is forward invariant for the flow of f, we extend the definition of circle-valued phase (see section A.3) to include continuous maps $\varphi : U \to \mathrm{S}^1 \subset \mathbb{C}$ satisfying $\varphi \circ \Phi_t = e^{i\omega t}\varphi$ for all $t \geq 0$. (We use this generality in the proof of theorem 3.) For the following lemmas and theorem, $d\theta$ denotes the standard angular form on the circle S^1 and $i = \sqrt{-1}$.

Lemma 2. *Consider an oscillator generated by the $\mathcal{C}^1$ vector field $f : \mathbf{M} \to \mathsf{T}\mathbf{M}$. Let U be a forward invariant open neighborhood of Γ. Given any $x_0 \in U$, there exists a unique circle-valued phase $\varphi : U \to \mathrm{S}^1$ satisfying $\varphi(x_0) = 1$. Moreover, $\varphi \in \mathcal{C}^{k\geq 1}$ if $f \in \mathcal{C}^k$.*

Proof. Existence follows by first defining $\varphi|_\Gamma : \Gamma \to \mathrm{S}^1$ by $\varphi|_\Gamma \circ \mathrm{P}(x_0) = 1$ and $\varphi|_\Gamma \circ \Phi_t = e^{i\omega t}\varphi|_\Gamma$, then defining $\varphi =: \varphi|_\Gamma \circ \mathrm{P}$. (As explained in section A.3, $\mathrm{P} \in \mathcal{C}^k$ when $f \in \mathcal{C}^k$.) To show uniqueness, let φ_1 and φ_2 be two such circle-valued phases. The ratio φ_1/φ_2 is constant along trajectories of f, so φ_1/φ_2 is constant on Γ. Since all trajectories converge to Γ, it follows from continuity that $\varphi_1/\varphi_2 \equiv \varphi_1(x_0)/\varphi_2(x_0) = 1$ on U, so $\varphi_1 = \varphi_2$ as desired. □

Lemma 3. *Consider an oscillator generated by the $\mathcal{C}^1$ vector field $f : \mathbf{M} \to \mathsf{T}\mathbf{M}$. Let U be a forward invariant open neighborhood of Γ, and let β be any $\mathcal{C}^{k\geq 0}$ closed 1-form on U satisfying $\langle \beta, f\rangle \equiv \omega$. Then for any $x_0 \in U$, there is a unique $\mathcal{C}^{k+1}$ circle-valued phase $\varphi : U \to \mathrm{S}^1$ satisfying $\varphi(x_0) = 1$ and $\varphi^*(d\theta) = \beta$.*

Downloaded from http://direct.mit.edu/neco/article-pdf/37/12/2158/2554618/neco.a.32.pdf by Ramona Marchand on 07 December 2025

Proof. Since U is forward invariant, it follows that Γ is a deformation retraction of U.[9] Since β is closed and satisfies $\langle \beta, f \rangle \equiv \omega$, it follows that the line integral of β along any continuous closed curve in U is an integer multiple of 2π. Thus, exponentiating i times the line integrals of β along arbitrary continuous paths from x_0 defines a $\mathcal{C}^{k+1}$ map $\varphi : U \to \mathrm{S}^1$ satisfying $\beta = \varphi^*(d\theta)$ (see the proof in Pajitnov, 2006, lemma 1.17). Moreover, the condition $\langle \beta, f \rangle \equiv \omega$ implies that φ is a circle-valued phase. The uniqueness of φ follows from lemma 2. □

The following result summarizes some relationships between different representations of asymptotic phase.

Theorem 1. *Consider an oscillator generated by the $\mathcal{C}^1$ vector field $f : \mathbf{M} \to \mathsf{T}\mathbf{M}$, with an asymptotic phase map denoted by $\mathrm{P} : \mathbf{M} \to \Gamma$.*

1. *The Temporal 1-Form $d\phi$ is the unique continuous closed 1-form on $\mathbf{M}$ satisfying*

$$\langle d\phi, f \rangle \equiv \omega.$$

2. *If φ is any circle-valued phase, $\varphi \circ \mathrm{P} = \varphi$ and*

$$d\phi = \varphi^*(d\theta) = -i(\mathbf{d}\varphi)/\varphi.$$

3. *Conversely, a choice of $x_0 \in \mathbf{M}$ uniquely determines a circle-valued phase φ satisfying $\varphi(x_0) = 1$ through the formula*

$$\varphi(x) = \exp\left(i \int_\gamma d\phi\right), \tag{A.9}$$

where γ is any $\mathcal{C}^0$ path joining x_0 to x.

Proof. Claim 3 is immediate from lemma 3 and its proof (taking $U = \mathbf{M}$). The first statement of claim 2 follows since $\varphi \circ \mathrm{P}$ and φ are both circle-valued phases agreeing on Γ (since $\mathrm{P}|_\Gamma = \mathrm{id}|_\Gamma$), so they coincide by lemma 2.

Since any two circle-valued phases differ by a rotation of S^1 (lemma 2), and since $d\theta$ is rotation invariant, lemma 3 implies claim 1 and the equality $d\phi = \varphi^*(d\theta)$ in claim 2. The remaining equality in claim 2 follows from the straightforward verification that $\varphi^*(d\theta) = -i(\mathbf{d}\varphi)/\varphi$ for any $\mathcal{C}^1$ circle-valued map φ, where $\mathbf{d}\varphi$ is viewed as a complex-valued differential 1-form (Guillemin & Pollack, 2010, p. 192). □

[9] In fact, it is a strong deformation retract. As an embedded submanifold of U, the limit cycle is a strong deformation retract of a "tubular neighborhood" (Lee, 2013) containing it. Using the flow, one may construct a strong deformation retract of U onto a tubular neighborhood. Following this homotopy with the strong deformation retraction of the tubular neighborhood onto the limit cycle then gives the desired strong deformation retraction.

Downloaded from http://direct.mit.edu/neco/article-pdf/37/12/2158/2554618/neco.a.32.pdf by Ramona Marchand on 07 December 2025

A.5 The Temporal 1-Form Estimated from Uncertain Systems. In this section, we prove two theorems relating the performance of the true Temporal 1-Form to that of estimates computed in the presence of noise, to which data from real-world systems and measurements are subjected. These are extensions of corresponding results in Kvalheim (2018).

Throughout the remainder of this section, we assume for simplicity that the state space $\mathbf{M}$ (also assumed to be the basin of attraction of the limit cycle) is an open subset of $\mathbb{R}^n$. We also assume for the remainder of this section that data take values in a fixed compact set $K \subset \mathbf{M}$.

In what follows, we let $\|\cdot\|$ be the Euclidean norm, and we denote induced operator norms by the same symbol. Given a continuous function β on a set $A \subset \mathbf{M}$, we define

$$\|\beta\|_{\mathcal{C}^0(A)} =: \sup_{x \in A} \|\beta(x)\|.$$

We denote by $\Omega^1_0(A)$ the set of continuous 1-forms over A, that is, continuous sections of $\mathsf{T}^*\mathbf{M}|_A$.

A.5.1 Assumptions about Data and Noise. We assume that we have a finite collection of pairs $(x_i, \dot{x}_i)_{i=1}^N \subset K \times \mathbb{R}^n$, with $\dot{x}_i$ of the form $\dot{x}_i = f(x_i) + \eta_i$. We consider the $x_i \in K$ and $\eta_i \in \mathbb{R}^n$ to be random variables, and we assume that there is a constant $\kappa \geq 0$ such that

$$\forall i : \mathbb{E}(\|\eta_i\|^2) \leq \kappa. \tag{A.10}$$

We also assume that the strong law of large numbers applies to yield the following equality with probability 1; quite general conditions ensuring this can be found in Doob (1990), Andrews (1987), and Pötscher and Prucha (1989).

$$\lim_{N \to \infty} \frac{1}{N} \sum_{i=1}^{N} \|\eta_i\|^2 - \mathbb{E}(\|\eta_i\|^2) \overset{\text{a.s.}}{=} 0 \tag{A.11}$$

We impose additional conditions involving the x_i for theorem 3 but not for theorem 2.

Remark 1. This setup is sufficiently general that the η_i could arise from measurement noise, or system noise, or both. Kvalheim (2018) argues in detail that this formulation applies to data from Itô SDEs. It also applies to data coming from Stratonovich SDEs, but there is a slight twist: to get sharper results, one should replace f by a modified vector field related to Itô's formula (Kvalheim, 2018).

Downloaded from http://direct.mit.edu/neco/article-pdf/37/12/2158/2554618/neco.a.32.pdf by Ramona Marchand on 07 December 2025

A.5.2 Performance of the Estimated Temporal 1-Form. Denote by $d\phi$, the unique true Temporal 1-Form on $\mathbf{M}$ corresponding to the vector field $f \in \mathcal{C}^1$. We define the "unobserved" cost function $J_N : \Omega_0^1(K) \to [0, \infty)$, which has $d\phi \in \mathcal{C}^0$ as its (nonunique) global minimizer, with minimum $J_N(d\phi) = 0$, by

$$J_N(\beta) := \frac{1}{N} \sum_{i=1}^{N} \left(\langle \beta(x_i),\, f(x_i) \rangle - \omega \right)^2 . \tag{A.12}$$

We also define the following "observed" cost function $\widehat{J_N} : \Omega_0^1(K) \to [0, \infty)$ by

$$\widehat{J_N}(\beta) := \frac{1}{N} \sum_{i=1}^{N} \left(\langle \beta(x_i),\, f(x_i) + \eta_i \rangle - \omega \right)^2 . \tag{A.13}$$

Fix $\epsilon \geq 0$. For each N we fix any $\widehat{d\phi}_N \in \Omega_0^1(K)$ with the property that

$$\widehat{J_N}\left(\widehat{d\phi}_N \right) \leq \widehat{J_N}(d\phi) + \epsilon. \tag{A.14}$$

We think of $\widehat{d\phi}_N$ as being the output of our algorithm to compute the Temporal 1-Form; our algorithm effectively attempts to minimize $\widehat{J_N}$. We have the following performance bound on our algorithm (assuming its output satisfies equation A.14) with respect to minimizing J_N.

Theorem 2. *Consider an oscillator generated by the $\mathcal{C}^1$ vector field $f : \mathbf{M} \to \mathsf{T}\mathbf{M}$. Then*

$$\frac{1}{4} \left(\frac{\sqrt{J_N(\widehat{d\phi}_N)} - 2\sqrt{\epsilon}}{\|d\phi\|_{\mathcal{C}^0(K)} + (1+\sqrt{2})\|\widehat{d\phi}_N\|_{\mathcal{C}^0(K)}} \right)^2 \leq \frac{1}{N} \sum_{i=1}^{N} \|\eta_i\|^2.$$

Thus, under the assumptions of this section,

$$\limsup_{N\to\infty} \frac{\sqrt{J_N(\widehat{d\phi}_N)} - 2\sqrt{\epsilon}}{\|d\phi\|_{\mathcal{C}^0(K)} + (1+\sqrt{2})\|\widehat{d\phi}_N\|_{\mathcal{C}^0(K)}} \overset{\text{a.s.}}{\leq} 2\sqrt{\kappa}.$$

In particular, if $\|d\phi\|_{\mathcal{C}^0(K)}, \|\widehat{d\phi}_N\|_{\mathcal{C}^0(K)} \leq M_0$, then

$$\limsup_{N\to\infty} \sqrt{J_N\left(\widehat{d\phi}_N\right)} \overset{\text{a.s.}}{\leq} \left(4 + 2\sqrt{2}\right) M_0 \sqrt{\kappa} + 2\sqrt{\epsilon}.$$

We make several remarks before giving the proof.

Downloaded from http://direct.mit.edu/neco/article-pdf/37/12/2158/2554618/neco.a.32.pdf by Ramona Marchand on 07 December 2025

Remark 2. The assumptions A.10 and A.11 are not needed for the first inequality of the theorem.

Remark 3 (Convergence rates). The first inequality in the theorem shows that the left side converges to $[0, \kappa]$ at least as fast as the rate of convergence in the law of large numbers see equation A.11. Similarly, with respect to the weak law of large numbers, the same inequality implies that the rate of convergence in probability of the left side is at least as fast as the corresponding rates of convergence in probability for the empirical second moments of the η_i. Similar remarks hold for equation A.25 in theorem 3.

Remark 4. The appearance of $\|d\phi\|_{\mathcal{C}^0(K)}$ in the first and second bounds suggests that a ("wilder") Temporal 1-Form with large supremum norm is harder to estimate. See also equation A.25 in theorem 3.

Remark 5. Since $d\phi \in \mathcal{C}^0$, there exists $M_0 > 0$ such that the assumption $\|d\phi\|_{\mathcal{C}^0(K)} \leq M_0$ holds. Since in practice the estimates $\widehat{d\phi}_N$ produced by our algorithm are uniformly bounded, for practical purposes, it is also the case that $\|\widehat{d\phi}\|_{\mathcal{C}^0(K)} \leq M_0$ for some M_0 and all N. Thus, the extra assumptions in the second portion of the theorem are quite mild.

Remark 6. Since $J_N(d\phi) = 0$, the estimate provided by theorem 2 bounds how well our algorithm does at minimizing the "unobserved" cost function. Taking $\epsilon = 0$ for simplicity, the final inequality of the theorem asserts that with f fixed, the performance of the estimator—as measured by J_N—is asymptotically within $\mathcal{O}(\kappa)$ of optimality. However, theorem 2 does not say anything about how close the estimate $\widehat{d\phi}_N$ itself is to the true Temporal 1-Form $d\phi$. This will be addressed in theorem 3.

Proof of Theorem 2. Expanding the summand in the definition of $\widehat{J_N}$ and rearranging, we see that for any $\beta \in \Omega^1_0(K)$:

$$\begin{aligned} J_N(\beta) &= \widehat{J_N}(\beta) - \frac{1}{N}\sum_{i=1}^{N} \langle \beta(x_i), \eta_i \rangle^2 \\ &\quad - \frac{2}{N}\sum_{i=1}^{N} \left(\langle \beta(x_i), f(x_i) \rangle - 1 \right) \langle \beta(x_i), \eta_i \rangle \qquad \text{(A.15)} \\ &\leq \widehat{J_N}(\beta) + 2\,[J_N(\beta)]^{\frac{1}{2}} \left[\frac{1}{N}\sum_{i=1}^{N} \langle \beta(x_i), \eta_i \rangle^2 \right]^{\frac{1}{2}} \\ &\quad + \frac{1}{N}\sum_{i=1}^{N} \langle \beta(x_i), \eta_i \rangle^2 , \qquad \text{(A.16)} \end{aligned}$$

where the inequality follows from the Cauchy-Schwarz inequality. Since the true Temporal 1-Form $d\phi$ satisfies $(\langle d\phi, f \rangle - 1) \equiv 0$, it follows immediately

Downloaded from http://direct.mit.edu/neco/article-pdf/37/12/2158/2554618/neco.a.32.pdf by Ramona Marchand on 07 December 2025

from equation A.15 that

$$\widehat{J_N}(d\phi) = \frac{1}{N}\sum_{i=1}^{N} \left\langle d\phi(x_i), \eta_i \right\rangle^2 . \tag{A.17}$$

Next, equations A.14 and A.16 imply that

$$\begin{aligned} J_N\left(\widehat{d\phi}_N\right) \leq \epsilon + \widehat{J_N}(d\phi) + \frac{1}{N}\sum_{i=1}^{N} \left\langle \widehat{d\phi}_N(x_i), \eta_i \right\rangle^2 \\ + 2\left[J_N\left(\widehat{d\phi}_N\right)\right]^{\frac{1}{2}} \left[\frac{1}{N}\sum_{i=1}^{N} \left\langle \widehat{d\phi}_N(x_i), \eta_i \right\rangle^2\right]^{\frac{1}{2}} . \end{aligned} \tag{A.18}$$

Defining $S_N, T_N \geq 0$ by

$$S_N^2 =: \frac{1}{N}\sum_{i=1}^{N} \|\eta_i\|^2, \quad T_N^2 =: J_N\left(\widehat{d\phi}_N\right),$$

substituting equation A.17 into A.18, and using Cauchy-Schwarz yields an inequality quadratic in T_N:

$$\begin{aligned} T_N^2 - 2S_N \left\|\widehat{d\phi}_N\right\|_{\mathcal{C}^0(K)} T_N - \left(\|d\phi\|_{\mathcal{C}^0(K)}^2 + \left\|\widehat{d\phi}_N\right\|_{\mathcal{C}^0(K)}^2\right) S_N^2 \\ \leq \epsilon . \end{aligned}$$

This and the quadratic formula imply that

$$\begin{aligned} T_N \leq 2S_N \left\|\widehat{d\phi}_N\right\|_{\mathcal{C}^0(K)} \\ + 2\left[\left(\|d\phi\|_{\mathcal{C}^0(K)}^2 + 2\left\|\widehat{d\phi}_N\right\|_{\mathcal{C}^0(K)}^2\right) S_N^2 + \epsilon\right]^{\frac{1}{2}} . \end{aligned}$$

Using subadditivity of $\sqrt{\cdot}$, squaring, and rearranging yields

$$\frac{T_N - 2\sqrt{\epsilon}}{\|d\phi\|_{\mathcal{C}^0(K)} + \left(1+\sqrt{2}\right)\left\|\widehat{d\phi}_N\right\|_{\mathcal{C}^0(K)}} \leq 2S_N .$$

This yields the first inequality of the theorem statement; taking the lim sup of both sides as $N \to \infty$ and using equations A.10 and A.11 completes the proof. □

Downloaded from http://direct.mit.edu/neco/article-pdf/37/12/2158/2554618/neco.a.32.pdf by Ramona Marchand on 07 December 2025

We now begin preparations for the statement of theorem 3. Fix a compact subset $\mathcal{E} \subset \Omega_0^1(K)$[10] and define

$$\mathcal{F} := \{\beta \in \mathcal{E} | \beta \text{ is closed}\}.$$

It follows that $\mathcal{F}$ is compact since it is closed in $\Omega_0^1(K)$. This follows since the limit in $\Omega_0^1(K)$ of a sequence $(\beta_i) \subset \mathcal{F}$ must have integral zero over any nullhomotopic continuous loop in K, since the same is true of each β_i, so the limit is a closed 1-form.

For theorem 3, we assume that the strong uniform law of large numbers applies to yield

$$\lim_{N\to\infty} \sup_{\beta\in\mathcal{F}} \left| J_N(\beta) - \int_K (\langle \beta, f\rangle - \omega)^2 \rho d\mu \right|, \stackrel{\text{a.s.}}{=} 0, \tag{A.19}$$

where μ is some Borel probability measure on K. Quite general conditions ensuring this can be found in Andrews (1987) and Pötscher and Prucha (1989). Recall that the "support" of a Borel measure μ is the set of all points x such that every neighborhood of x has positive measure.

We first need to prove the following lemma, in which aff($\cdot$) denotes the "affine hull" of a subset of $\Omega_0^1(K)$.

Lemma 4. *Consider an oscillator generated by the $\mathcal{C}^1$ vector field $f : \mathbf{M} \to \mathsf{T}\mathbf{M}$. Assume that $U \subset K$ is an open neighborhood of Γ in $\mathbf{M}$, which is forward invariant and contained in the support of μ. Also assume that $d\phi \in \mathcal{F}$, that $\mathcal{F}$ is star-shaped with respect to $d\phi$, and that there is $\delta > 0$ such that*

$$\forall \beta \in \text{aff}(\mathcal{F}) : \|\beta - d\phi\|_{\mathcal{C}^0(U)} \leq \delta \Longrightarrow \beta \in \mathcal{F}. \tag{A.20}$$

Then there is $c > 0$ such that, for all $\beta \in -d\phi + \mathcal{F}$,

$$c\|\beta\|^2_{\mathcal{C}^0(U)} \leq \int_U \langle \beta, f\rangle^2 d\mu. \tag{A.21}$$

Remark 7. A stronger assumption implying the star-shaped hypothesis is that $\mathcal{F}$ is convex, since then $\mathcal{F}$ is star shaped with respect to all points in $\mathcal{F}$.

Proof. Define $Q : \Omega_0^1(K) \to [0, \infty)$ to send β to the right side of equation A.21, $\tilde{\mathcal{F}} =: -d\phi + \mathcal{F}$, and

[10] Note that by the Arzelà-Ascoli theorem, the compact subsets of $\Omega_0^1(K)$ are precisely the closed and bounded subsets of 1-forms, which are equicontinuous.

Downloaded from http://direct.mit.edu/neco/article-pdf/37/12/2158/2554618/neco.a.32.pdf by Ramona Marchand on 07 December 2025

$$B =: \{\beta \in \text{aff}(\tilde{\mathcal{F}}) : \|\beta\|_{\mathcal{C}^0(U)} = \delta\}. \tag{A.22}$$

Since $\mathcal{F}$ is compact and star shaped with respect to $d\phi$, it follows that $\tilde{\mathcal{F}}$ is compact and star shaped with respect to 0. Since Q is continuous and B is compact (by equation A.20), $Q|_B$ attains a minimum $c_0 \geq 0$.

We claim that $c_0 > 0$. Indeed, $Q(\beta) = 0$ implies that $\langle \beta|_U, f|_U \rangle \equiv 0$, which implies that $\beta|_U = dh$ for some $\mathcal{C}^1$ function $h : U \to \mathbb{R}$ constant along the flow of f. But h must be constant everywhere since all trajectories converge to Γ, so $\|\beta\|_{\mathcal{C}^0(U)} = 0$. This and equation A.22 imply that $\beta \notin B$, so $c_0 > 0$.

Since $\tilde{\mathcal{F}}$ is star shaped with respect to 0, each nonzero $\beta \in \tilde{\mathcal{F}}$ is of the form $t\gamma$ for some $\gamma \in B$ and $t =: \|\beta\|_{\mathcal{C}^0(U)}/\delta$. Since $Q(t\gamma) = t^2 Q(\gamma) \geq t^2 c_0$, it follows that $Q(\beta) \geq \|\beta\|^2_{\mathcal{C}^0(U)} c_0/\delta^2$ for all $\beta \in \tilde{\mathcal{F}}$. Defining $c =: c_0/\delta^2$ completes the proof. □

Theorem 3. *Consider an oscillator generated by the $\mathcal{C}^1$ vector field $f : \mathbf{M} \to \mathbf{TM}$. Assume that $U \subset K$ is an open neighborhood of Γ in $\mathbf{M}$, which is forward invariant and contained in the support of μ. Also assume that $\widehat{d\phi}_N, d\phi \in \mathcal{F}$. Then, under the assumptions of this section,*

$$\lim_{\kappa+\epsilon\to 0} \limsup_{N\to\infty} \left\|\widehat{d\phi}_N - d\phi\right\|_{\mathcal{C}^0(U)} \overset{\text{a.s.}}{=} 0. \tag{A.23}$$

If also $\mathcal{F}$ is star shaped with respect to $d\phi$, equation A.20 holds for some $\delta > 0$, and $\zeta, \xi : \mathbb{N} \to [0, \infty)$ satisfy

$$\begin{aligned} &\frac{1}{N}\sum_{i=1}^{N} \|\eta_i\|^2 \leq \zeta(N) \\ &\left| J_N\left(\widehat{d\phi}_N\right) - \int_K \left(\langle \widehat{d\phi}_N, f\rangle - \omega\right)^2 \rho d\mu \right| \leq \xi(N), \end{aligned} \tag{A.24}$$

then the following explicit convergence rates hold:

$$\begin{aligned} &c\left\|\widehat{d\phi}_N - d\phi\right\|^2_{\mathcal{C}^0(U)} \\ &\leq \xi(N) + 4\left[\left(\|d\phi\|_{\mathcal{C}^0(K)} + \left(1+\sqrt{2}\right)\left\|\widehat{d\phi}_N\right\|_{\mathcal{C}^0(K)}\right)\zeta(N) + \sqrt{\epsilon}\right]^2 \\ &\leq \xi(N) + 4\left[\left(2+\sqrt{2}\right)M_0\zeta(N) + \sqrt{\epsilon}\right]^2, \end{aligned} \tag{A.25}$$

where $c > 0$ is the constant in lemma 4, and the final inequality holds if $\|d\phi\|_{\mathcal{C}^0(K)}, \|\widehat{d\phi}_N\|_{\mathcal{C}^0(K)} \leq M_0$.

We make several remarks before giving the proof.

Downloaded from http://direct.mit.edu/neco/article-pdf/37/12/2158/2554618/neco.a.32.pdf by Ramona Marchand on 07 December 2025

Remark 8. As noted in remark 7, the star-shaped hypothesis is automatic if $\mathcal{F}$ is convex.

Remark 9. The assumption equation A.19 is not needed for the second portion of the theorem, since its role is replaced by equation A.24.

Remark 10. Unlike theorem 2, theorem 3 gives which the estimates $\widehat{d\phi}_N$ converge to the true Temporal 1-Form $d\phi$ uniformly on suitable neighborhoods $U \subset K$ of Γ. This convergence implies convergence of the corresponding isochron estimates to the true isochrons $\mathcal{C}^1$-uniformly on such neighborhoods. This implies, roughly speaking, that the estimated isochrons corresponding to $\widehat{d\phi}_N$ will resemble the true isochrons near Γ up to one order of smoothness.

Remark 11. For nonforward invariant U, the conclusions of the theorem do not generally hold because it is possible to construct examples of such a U on which there are many closed 1-forms β satisfying $\langle \beta, f \rangle \equiv \omega$, and this nonuniqueness makes it possible to construct examples violating the conclusions of the theorem. However, given some curious apparent experimental successes with nonforward invariant U (see the guinea fowl example of Figure 6), it would be interesting to know whether something useful can be said about a subclass of open sets U strictly larger than those considered in the theorem.

Remark 12. When $f \in \mathcal{C}^{k+1}$, it is possible to extend theorem 3 to obtain convergence in $\mathcal{C}^k$ norm rather than merely $\mathcal{C}^0$ norm. The proof is nearly the same, but it requires additional care in defining function spaces (since K is an arbitrary compact subset of $\mathbf{M}$). We defer a careful treatment to future work.

Proof of Theorem 3. We first establish equation A.23. By equation A.19 with probability 1, the function $J_N|_{\mathcal{F}} : \mathcal{F} \to [0, \infty)$ converges uniformly to the continuous function $J : \mathcal{F} \to [0, \infty)$ defined by

$$J(\beta) =: \int_K (\langle \beta, f \rangle - \omega)^2 \, d\mu.$$

Hence,

$$\limsup_{N \to \infty} J\left(\widehat{d\phi}_N\right) \overset{\text{a.s.}}{=} \limsup_{N \to \infty} J_N\left(\widehat{d\phi}_N\right),$$

so theorem 2 implies that

$$\lim_{\kappa + \epsilon \to 0} \limsup_{N \to \infty} J\left(\widehat{d\phi}_N\right) \overset{\text{a.s.}}{=} 0.$$

Defining $\mathcal{M}$ to be the set of global minimizers of $J|_{\mathcal{F}}$ (attaining the minimum value of 0) and using compactness of $\mathcal{F}$, it follows that

Downloaded from http://direct.mit.edu/neco/article-pdf/37/12/2158/2554618/neco.a.32.pdf by Ramona Marchand on 07 December 2025

$$\lim_{\kappa+\epsilon\to 0} \limsup_{N\to\infty} d\left(\widehat{d\phi}_N, \mathcal{M}\right)_{\mathcal{C}^0(K)} \overset{\text{a.s.}}{=} 0,$$

where $d(\alpha, \mathcal{M})_{\mathcal{C}^0(K)} =: \inf_{\beta\in\mathcal{M}} \|\alpha - \beta\|_{\mathcal{C}^0(K)}$. (See the Berge maximum theorem (Aliprantis & Border, 2006, theorem 17.31).)

Thus, to complete the proof of equation A.23, it suffices to show that the restriction to U of every closed 1-form in $\mathcal{M}$ coincides with $d\phi|_U$. Since J has minimum 0 and U is contained in the support of μ, it follows that any $\beta \in \mathcal{M}$ must satisfy $\langle \beta, f\rangle \equiv \omega$. Since U is forward invariant, the same argument as in the final paragraph of the proof of theorem 1 (using lemmas 2 and 3) then implies that $\beta = d\phi|_U$, as desired.

Next, assume that $\mathcal{F}$ is star shaped with respect to $d\phi$, equation A.20 holds for some $\delta > 0$, and equation A.24 holds. Defining $\beta_N =: \widehat{d\phi}_N - d\phi \in -d\phi + \mathcal{F}$ for each N, lemma 4 implies the first inequality below:

$$\begin{aligned} c\|\beta_N\|^2_{\mathcal{C}^0(U)} &\le \int_U \langle \beta_N, f\rangle^2 d\mu \\ &\le \int_K \langle \beta_N, f\rangle^2 d\mu = J\left(\widehat{d\phi}_N\right). \end{aligned} \tag{A.26}$$

The second inequality follows from $U \subset K$, and the equality follows from expanding the integrand defining J. On the other hand, theorem 2 implies that

$$\frac{1}{4}\left(\frac{\sqrt{J_N(\widehat{d\phi}_N)} - 2\sqrt{\epsilon}}{\|d\phi\|_{\mathcal{C}^0(K)} + (1+\sqrt{2})\|\widehat{d\phi}_N\|_{\mathcal{C}^0(K)}}\right)^2 \le \frac{1}{N}\sum_{i=1}^{N}\|\eta_i\|^2.$$

Rearranging and using equations A.24 and A.26 yields the first inequality in equation A.25. The second inequality in equation A.25 follows directly from this and $\|d\phi\|_{\mathcal{C}^0(K)}, \|\widehat{d\phi}_N\|_{\mathcal{C}^0(K)} \le M_0$. □

Appendix B: Commonly Used Symbols

Symbol	Description/Meaning
$\dot{x}$	Time derivative of x
ω	Angular frequency
ϕ	A phase
$\mathbf{d}$	Exterior derivative
$\mathsf{T}A$	Tangent space of A
x^T	Transpose of x
r	Radial coordinate
θ	Angular coordinate
z	Out of plane coordinates
v_ν	Basis function

Downloaded from http://direct.mit.edu/neco/article-pdf/37/12/2158/2554618/neco.a.32.pdf by Ramona Marchand on 07 December 2025

Γ	Limit cycle
$\mathbf{M}$	A manifold
η	A noise process
$\mathrm{d}\theta$	Differential of angle θ
φ	Circle-valued phase
J_N	Cost function
q	Rectified coordinates
$\widehat{J_N}$	Estimated cost function
m_μ	Coefficient in series expansion for $\mathrm{d}\phi$
$v_\mu(\theta, r, z)$	Basis function in rectified coordinates
$u_k(\theta)$	Fourier basis function in angle
$\rho_j(r)$	Polynomial basis function in radius
$\xi_i(z)$	Out-of-plane basis function in z
$\mathrm{d}v_\mu$	Differential of sum of basis function v_μ

Acknowledgments

We are deeply indebted to John M. Guckenheimer for conceiving of the temporal 1-form and providing guidance and comments. We also thank Dan Guralnik and G. Bard Ermentrout for valuable insights. This work was supported by EPSRC grant EP/H04924X/1, BBSRC grant BB/J021504/1, and U S Army Research Office under contract/grant number 64929EG supporting S. Wilshin; ARO W911NF-18-1-0327 and ONR N000141612817 (held by D. E. Koditschek) supporting M. D. Kvalheim; NSF grants 1422157 1838179 to C. Scott; ARO Young Investigator Award 61770, W911NF-14-1-0573, D. Dan & Betty Kahn Foundation Autonomous Systems Megaproject, NSF CPS 2038432, ARO MURI W911NF-17- 1-0306, & NSF CMMI 1825918 to S. Revzen. The guinea fowl kinematics were gathered under the supervision of M. Daley with the support of a Human Frontier Science Program grant (RGY0062/2010) and ethical approval was obtained from the Royal Veterinary College Ethics and Welfare Committee under the protocol title, "Kinematics and Kinetics in Birds Running over Uneven Terrain." The optical transmission data for the Belousov-Zhabotinsky reaction were obtained from S. Fraden and M. Norton of Brandeis University, under awards from the National Science Foundation, NSF DMREF-1534890, and US Army Research Laboratory and US Army Research Office W911NF-16-1-0094.

References

Aliprantis, C. D., & Border, K. C. (2006). *Infinite dimensional analysis* (3rd ed.). Springer.

Ames, A. D., & Sastry, S. (2005). A homology theory for hybrid systems: Hybrid homology. In *Proceedings of the International Workshop on Hybrid Systems: Computation and Control* (pp. 86–102).

Downloaded from http://direct.mit.edu/neco/article-pdf/37/12/2158/2554618/neco.a.32.pdf by Ramona Marchand on 07 December 2025

Andrews, D. W. K. (1987). Consistency in nonlinear econometric models: A generic uniform law of large numbers. *Econometrica*, *55*(6), 1465–1471. 10.2307/1913568

Ankarali, M. M., & Cowan, N. J. (2014). System identification of rhythmic hybriddynamical systems via discrete time harmonic transfer functions. In *Proceedings of the 53rd IEEE Conference on Decision and Control* (pp. 1017–1022).

Arnold, L. (1974). *Stochastic differential equations: Theory and applications*. Wiley.

Back, A., Guckenheimer, J., & Myers, M. (1993). A dynamical simulation facility for hybrid systems. In R. Grossman & A. Rischel (Eds.), *Hybrid systems* (pp. 255–267). Springer.

Bagheri, S. (2014). Effects of weak noise on oscillating flows: Linking quality factor, floquet modes, and Koopman spectrum. *Physics of Fluids*, *26*(9). 10.1063/1.4895898

Bastani, A. F., & Hosseini, S. M. (2007). A new adaptive Runge-Kutta method for stochastic differential equations. *Journal of Computational and Applied Mathematics*, *206*(2), 631–644. 10.1016/j.cam.2006.08.012

Briers, M., Doucet, A., & Maskell, S. (2009). Smoothing algorithms for state–space models. *Annals of the Institute of Statistical Mathematics*, *62*(1), 61.

Brunton, S. L., Budišić M., Kaiser, E., & Kutz, J. N. (2021). *Modern Koopman theory for dynamical systems*. arXiv:2102.12086.

Burrage, P. M. (1999). *Runge-Kutta methods for stochastic differential equations*. PhD diss., University of Queensland.

Cao, A., Lindner, B., & Thomas, P. J. (2020). A partial differential equation for the mean-return-time phase of planar stochastic oscillators. *SIAM Journal of Applied Mathematics*, *80*(1), 422–447. 10.1137/18M1218601

Cestnik, R., & Abel, M. (2019). Inferring the dynamics of oscillatory system using recurrent neural networks. *Chaos*, *29*(6).

Clark, W., & Bloch, A. (2021). *Invariant forms in hybrid and impact systems*. arXiv:2101.11128.

Colbrook, M. J. (2024). The multiverse of dynamic mode decomposition algorithms. In S. Mishra and A. Townsend (Eds.). *Numerical analysis meets machine learning* (pp. 127–230). Elsevier.

Cruse, H., & Schwarze, W. (1988). Mechanisms of coupling between the ipsilateral legs of a walking insect (*Carausius morosus*). *Journal of Experimental Biology*, *138*, 455–469. 10.1242/jeb.138.1.455

Danner, S. M., Hofstoetter, U. S., Freundl, B., Binder, H., Mayr, W., Rattay, F., & Minassian, K. (2015). Human spinal locomotor control is based on flexibly organized burst generators. *Brain*, *138*(3), 577–588. 10.1093/brain/awu372

de Rham, G. (1984). *Differentiable manifolds*. Springer-Verlag.

Doob, J. L. (1990). *Stochastic processes*. Wiley.

Duffing, G. (1918). *Erzwungene Schwingungen bei veränderlicher Eigenfrequenz undihre technische Bedeutung*. R. Vieweg & Sohn.

Eldering, J., Kvalheim, M., & Revzen, S. (2018). Global linearization and fiber bundle structure of invariant manifolds. *Nonlinearity*, *31*(9), 4202–4245. 10.1088/1361-6544/aaca8d

Engel, M., & Kuehn, C. (2021). A random dynamical systems perspective onisochronicity for stochastic oscillations. *Communications in Mathematical Physics*, *386*(3), 1603–1641. 10.1007/s00220-021-04077-z

Downloaded from http://direct.mit.edu/neco/article-pdf/37/12/2158/2554618/neco.a.32.pdf by Ramona Marchand on 07 December 2025

Epstein, I. R., & Pojman, J. A. (1998). *An introduction to nonlinear chemical dynamics: Oscillations, waves, patterns, and chaos*. Oxford University Press.

Ermentrout, B. (1996). Type 1 membranes, phase resetting curves, and synchrony. *Neural Computation*, *8*(5), 979–1001. 10.1162/neco.1996.8.5.979

Evans, L. C. (2013). *An introduction to stochastic differential equations*. American Mathematical Society.

Farber, M., Kappeler, T., Latschev, J., & Zehnder, E. (2004). Lyapunov 1-forms for flows. *Ergodic Theory and Dynamical Systems*, *24*(5), 1451–1475. 10.1017/S0143385703000762

FitzHugh, R. (1961). Impulses and physiological states in theoretical models of nerve membrane. *Biophysical Journal*, *1*(6), 445–466. 10.1016/S0006-3495(61)86902-6

Floquet, G. (1883). Sur les équations différentielles linéaires à coefficients périodiques. *Annales Scientifiques de lÉcole Normale Supérieure, Sér*, *2*, 12.

Gardiner, C. W. (2004). *Handbook of stochastic methods* (3rd ed.). Springer-Verlag.

Gibson, J. F., Farmer, J. D., Casdagli, M., & Eubank, S. (1992). An analytic approach to practical state space reconstruction. *Physica D: Nonlinear Phenomena*, *57*(1–2), 1–30. 10.1016/0167-2789(92)90085-2

Głazek, S. D., & Wilson, K. G. (2002). Limit cycles in quantum theories. *Physical Review Letters*, *89*(23), 230–401.

Goebel, R., Sanfelice, R. G., & Teel, A. (2009). Hybrid dynamical systems. *Control Systems, IEEE*, *29*(2), 28–93. 10.1109/MCS.2008.931718

Guckenheimer, J. (1975). Isochrons and phaseless sets. *Journal of Mathematical Biology*, *1*, 259–273. 10.1007/BF01273747

Guillemin, V., & Pollack, A. (2010). *Differential topology*. AMS Chelsea Publishing.

Hénon, M. (1976). A two-dimensional mapping with a strange attractor. *Communications in Mathematical Physics*, *50*(1), 69–77.

Hirsch, M. W. (1976). *Differential topology*. Springer-Verlag.

Hirsch, M. W., Pugh, C. C., & Shub, M. (1977). *Invariant manifolds*. Springer-Verlag.

Hoppensteadt, F. C., & Izhikevich, E. M. (1997). *Weakly connected neural networks*. Springer-Verlag.

Huguet, G., & de la Llave, R. (2012). *Computation of limit cycles and their isochrones: Fast algorithms and their convergence*. Technical report 2415, Institute for Mathematics and Its Applications, University of Minnesota.

Jindrich, D. L., & Full, R. J. (2002). Dynamic stabilization of rapid hexapedal locomotion. *Journal of Experimental Biology*, *205*(18), 2803–2823. 10.1242/jeb.205.18.2803

Kostelich, E. J., & Yorke, J. A. (1990). Noise reduction: Finding the simplest dynamical system consistent with the data. *Physica D: Nonlinear Phenomena*, *41*, 183–196. 10.1016/0167-2789(90)90121-5

Kutz, J. N., Brunton, S. L., Brunton, B. W., & Proctor, J. L. (2016). *Dynamic mode decomposition: Data-driven modeling of complex systems*. SIAM.

Kvalheim, M. (2018). *Aspects of invariant manifold theory and applications*. PhD diss., University of Michigan.

Kvalheim, M. D., Gustafson, P., & Koditschek, D. E. (2021). Conley's fundamental theorem for a class of hybrid systems. *SIAM Journal on Applied Dynamical Systems*, *20*(2), 784–825. 10.1137/20M1336576

Downloaded from http://direct.mit.edu/neco/article-pdf/37/12/2158/2554618/neco.a.32.pdf by Ramona Marchand on 07 December 2025

Kvalheim, M. D., Hong, D., & Revzen, S. (2021). Generic properties of Koopman eigenfunctions for stable fixed points and periodic orbits. *IFAC-PapersOnLine*, *54*(9), 267–272. 10.1016/j.ifacol.2021.06.150

Kvalheim, M. D., & Revzen, S. (2021). Existence and uniqueness of global Koopman eigenfunctions for stable fixed points and periodic orbits. *Physica D*, *425*, 132959. 10.1016/j.physd.2021.132959

Langfield, P., Krauskopf, B., & Osinga, H. M. (2014). Solving Winfree's puzzle: The isochrons in the FitzhughNagumo model. *Chaos*, *24*(1), 013131. 10.1063/1.4867877

Langfield, P., Krauskopf, B., & Osinga, H. M. (2015). Forward-time and backward-time isochromes and their interactions. *SIAM Journal on Applied Dynamic Systems*, *14*(3), 1418–1453. 10.1137/15M1010191

Lee, J. M. (2013). *Introduction to smooth manifolds* (2nd ed.). Springer.

Lerman, E. (2016). *A category of hybrid systems*. arXiv:1612.01950.

Lerman, E., & Schmidt, J. (2020). Networks of hybrid open systems. *Journal of Geometry and Physics*, *149*, 103582. 10.1016/j.geomphys.2019.103582

Mauroy, A., & Mezić, I. (2012). On the use of Fourier averages to compute the global isochrons of (quasi) periodic dynamics. *Chaos*, *22*(3), 033112. 10.1063/1.4736859

Mauroy, A., & Mezić, I. (2018). Global computation of phase-amplitude reduction for limit-cycle dynamics. *Chaos*, *28*(7). 10.1063/1.5030175

Mauroy, A., Mezić, I., & Moehlis, J. (2013). Isostables, isochrons, and Koopman spectrum for the action–angle representation of stable fixed point dynamics. *Physica D: Nonlinear Phenomena*, *261*, 19–30. 10.1016/j.physd.2013.06.004

May, R. M. (1972). Limit cycles in predator-prey communities. *Science*, *177*(4052), 900–902. 10.1126/science.177.4052.900

Monga, B., Wilson, D., Matchen, T., & Moehlis, J. (2019). Phase reduction and phase-based optimal control for biological systems: A tutorial. *Biological Cybernetics*, *113*(1), 11–46. 10.1007/s00422-018-0780-z

Nagumo, J., Arimoto, S., & Yoshizawa, S. (1962). An active pulse transmission line simulating nerve axon. *Proceedings of the IRE*, *50*(10), 2061–2070. 10.1109/JRPROC.1962.288235

Øksendal, B. (2013). *Stochastic differential equations* (6th ed.). Springer-Verlag.

Osinga, H., & Moehlis, J. (2010). Continuation-based computation of global isochrons. *SIAM Journal on Applied Dynamical Systems*, *9*, 1201. 10.1137/090777244

Pajitnov, A. V. (2006). *Circle-valued Morse theory*. Walter de Gruyter.

Pérez-Cervera, A., & Huguet, G. (2020). Global phase-amplitude description of oscillatory dynamics via the parameterization method. *Chaos*, *30*(8), 083117.

Peters, J., & Schaal, S. (2008). Natural actor-critic. *Neurocomputing*, *71*(7–9), 1180–1190. 10.1016/j.neucom.2007.11.026

Pikovsky, A. (2015). Comment on "asymptotic phase for stochastic oscillators." *Physical Review Letters*, *115*(6), 069401.

Pötscher, B. M., & Prucha, I. R. (1989). A uniform law of large numbers for dependent and heterogeneous data processes. *Econometrica*, *57*(3), 675–683.

Rafiee, S., & Kiemel, T. (2020). Multiple strategies to correct errors in foot placement and control speed in human walking. *Experimental Brain Research*, *238*(12), 2947–2963. 10.1007/s00221-020-05949-x

Downloaded from http://direct.mit.edu/neco/article-pdf/37/12/2158/2554618/neco.a.32.pdf by Ramona Marchand on 07 December 2025

Revzen, S. (2009). *Neuromechanical control architectures in arthropod locomotion*. PhD diss., University of California, Berkeley.

Revzen, S., & Guckenheimer, J. M. (2008). Estimating the phase of synchronized oscillators. *Physical Review E*, *78*(5), 051907. 10.1103/PhysRevE.78.051907

Revzen, S., & Guckenheimer, J. M. (2012). Finding the dimension of slow dynamics in a rhythmic system. *Journal of the Royal Society Interface*, *9*(70), 957–971. 10.1098/rsif.2011.0431

Revzen, S., Guckenheimer, J. M., & Full, R. J. (2011). Subtle differences in gaits: The perspective of data driven floquet analysis. In *Proceedings of the Yearly Meeting of the Society for Integrative and Comparative Biology*.

Revzen, S., Koditschek, D. E., & Full, R. J. (2008). *Progress in motor control: A multidisciplinary perspective*. Springer Science + Business Media.

Revzen, S., & Kvalheim, M. (2015). Data driven models of legged locomotion. In *Proceedings of the Micro- and Nanotechnology Sensors, Systems, and Applications VII*. International Society for Optics and Photonics.

Revzen, S., & Kvalheim, M. (2016). Bioinspired legged locomotion. In *Locomotion as an oscillator* (pp. 97–108). Elsevier.

Sauer, T., Yorke, J. A., & Casdagli, M. (1991). Embedology. *Journal of Statistical Physics*, *65*(3–4), 579–616. 10.1007/BF01053745

Schaal, S., & Atkeson, C. (2010). Learning control in robotics. *Robotics and Automation Magazine*, *17*(2), 20–29. 10.1109/MRA.2010.936957

Schaal, S., Peters, J., Nakanishi, J., & Ijspeert, A. (2005). Learning movement primitives. In P. Sario & R. Chatila (Eds.), *Robotics research* (pp. 561–572). Springer-Verlag.

Schelter, B., Winterhalder, M., & Timmer, J. (Eds.). (2006). *Handbook of time series analysis: Recent theoretical developments and applications*. Wiley.

Schwabedal, J. T. C., & Pikovsky, A. (2013). Phase description of stochastic oscillations. *Physical Review Letters*, *11*(20), 204102.

Sel'Kov, E. E. (1968). Self-oscillations in glycolysis. *FEBS Journal*, *4*(1), 79–86.

Simić, S. N., Johansson, K. H., Sastry, S., & Lygeros, J. (2000). Toward a geometric theory of hybrid systems. In *Proceedings of the International Workshop on Hybrid Systems: Computation and Control* (pp. 421–436).

Spivak, M. (1971). *Calculus on manifolds*. Perseus.

Stoker, J. J. (1950). *Nonlinear vibrations in mechanical and electrical systems*. Interscience.

Takens, F. (1981). Detecting strange attractors in turbulence. In D. Rand & L. S. Young (Eds.), *Dynamical systems and turbulence* (pp. 366–381). Springer-Verlag.

Thomas, P. J., & Lindner, B. (2014). Asymptotic phase for stochastic oscillators. *Physical Review Letters*, *113*(*25*), 254101. 10.1103/PhysRevLett.113.254101

Thomas, P. J., & Lindner, B. (2015). Thomas & Lindner reply. *Physical Review Letters*, *115*(6), 069402. 10.1103/PhysRevLett.115.069402

Ting, L. H., Blickhan, R., & Full, R. J. (1994). Dynamic and static stability in hexapedal runners. *Journal of Experimental Biology*, *197*, 251–269. 10.1242/jeb.197.1.251

Tytell, E. D. (2013). The intrinsic dynamical properties of muscle are self-stabilizing for rhythmic movements. *Abstract at Annual Meeting of the Society for Integrative and Comparative Biology*.

Van der Pol, B. (1934). The nonlinear theory of electric oscillations. *Proceedings of the Institute of Radio Engineers*, *22*(9), 1051–1086.

Downloaded from http://direct.mit.edu/neco/article-pdf/37/12/2158/2554618/neco.a.32.pdf by Ramona Marchand on 07 December 2025

Wang, Y., & Srinivasan, M. (2012). System identification and stability analysis of steady human walking and the swing leg dynamics. In *Proceedings of the ASME 5th Annual Dynamic Systems and Control Conference*, vol. 2 (pp. 19–23).

Westervelt, E. R., Grizzle, J. W., & Koditschek, D. E. (2003). Hybrid zero dynamics of planar biped walkers. *IEEE Transactions on Automatic Control*, *48*(1), 42–56. 10.1109/TAC.2002.806653

Wilshin, S., Haynes, G. C., Porteous, J., Koditschek, D., Revzen, S., & Spence, A. J. (2017). Morphology and the gradient of a symmetric potential predict gait transitions of dogs. *Biological Cybernetics*, *111*(3), 269–277. 10.1007/s00422-017-0721-2

Wilshin, S., Kvalheim, M. D., & Revzen, S. (2021). *Phase response curves and the role of coordinates*. arXiv:2111.06511.

Wilshin, S., & Revzen, S. (2014). Phase driven models of unperturbed locomotion. *Integrative and Comparative Biology*, *54*.

Wilson, D. (2020). A data-driven phase and isostable reduced modeling framework for oscillatory dynamical systems. *Chaos*, *30*(1). 10.1063/1.5126122

Wilson, D., & Ermentrout, B. (2018). Greater accuracy and broadened applicability of phase reduction using isostable coordinates. *Journal of Mathematical Biology*, *76*, 37–66. 10.1007/s00285-017-1141-6

Winfree, A. T. (1980). *The geometry of biological time*. Springer-Verlag.

Wodeyar, A., Schatza, M., Widge, A. S., Eden, U. T., & Kramer, M. A. (2021). A state space modeling approach to real-time phase estimation. *eLife*, *10*, e68803. 10.7554/eLife.68803

Wu, Z., Brunton, S. L., & Revzen, S. (2021). Challenges in dynamic mode decomposition. *Journal of the Royal Society Interface*, *18*(185), 20210686. 10.1098/rsif.2021.0686

Received December 19, 2024; accepted June 12, 2025.

Downloaded from http://direct.mit.edu/neco/article-pdf/37/12/2158/2554618/neco.a.32.pdf by Ramona Marchand on 07 December 2025